

**Atomic cation-vacancy engineering of two-dimensional  
nanosheets for energy-related applications**

Journal:	<i>Materials Chemistry Frontiers</i>
Manuscript ID	QM-REV-11-2022-001166.R1
Article Type:	Review Article
Date Submitted by the Author:	15-Jan-2023
Complete List of Authors:	Liu, Chao; Nanjing University of Science and Technology Liu, Yifan; Nanjing University of Science and Technology Ma, Renzhi; National Institute for Materials Science, Soft Chemistry Group, Advanced Materials Laboratory Sasaki, Takayoshi; National Institute of Materials Science, International Center for Materials Nanoarchitectonics Wang, Xin; Nanjing University of Science and Technology, Xiong, Pan; Nanjing University of Science and Technology, School of Chemistry and Chemical Engineering Zhu, Junwu; Nanjing University of Science and Technology, Department of Chemical Engineering

## Atomic cation-vacancy engineering of two-dimensional nanosheets for energy-related applications

Chao Liu,<sup>†a</sup> Yifan Liu,<sup>†a</sup> Renzhi Ma,<sup>b</sup> Takayoshi Sasaki,<sup>\*b</sup> Xin Wang,<sup>a</sup> Pan Xiong<sup>\*a</sup> and Junwu Zhu<sup>\*a</sup>

Received 00th January 20xx,  
Accepted 00th January 20xx

DOI: 10.1039/x0xx00000x

Two-dimensional (2D) nanosheets delaminated from their layered parent crystals have shown great promise in energy-related applications, owing to their unique 2D features with atomic thickness, large specific surface area and tunable electronic properties. However, the performance of pristine 2D nanosheets is still insufficient for their further applications. Cation-vacancy engineering of 2D nanosheets is one of the most straightforward and effective approaches to improving their performance. Herein, the recent research progress in atomic cation-vacancy engineering of 2D nanosheets is reviewed, including layered transition metal oxide nanosheets, transition metal dichalcogenide nanosheets, layered double hydroxide nanosheets, transition metal carbide and nitride nanosheets, graphene, boron nitride and carbon nitride nanosheets. Various facile strategies are introduced for the incorporation of atomic-scale cation vacancies within these 2D nanosheets. The resulting superior electrochemical performances of these cation-deficient 2D nanosheets are discussed in detail for some typical energy-related applications, such as metal ion batteries, lithium-sulfur batteries, electrocatalysis and photocatalysis. Finally, the challenges and perspectives are outlined for future research.

### 1. Introduction

Two-dimensional (2D) materials have been extensively investigated for over a decade,<sup>1</sup> especially those unilamellar nanosheets delaminated from their layered parent crystals, including transition metal oxides/dichalcogenides,<sup>2-4</sup> layered double hydroxides (LDHs),<sup>5,6</sup> transition metal carbides and nitrides (MXenes).<sup>7,8</sup> Due to their unique 2D aspects such as atomic thickness, large specific surface area and tunable electronic properties, these 2D nanosheets show great promise in various energy-related applications. For instance, the graphene-based supercapacitor was first reported in 2008, which achieved a specific capacitance of 135 and 99 F/g in aqueous and organic electrolytes, respectively.<sup>9</sup> The MoS<sub>2</sub> nanosheets delivered the superior hydrogen evolution reaction (HER) activity with an overpotential of about 320 mV at 10 mA cm<sup>-2</sup>, owing to their edge site activities and accessibility.<sup>10</sup> However, the reported performance of these pristine 2D nanosheets is still insufficient for their practical applications. Many strategies have been explored to improve the properties of 2D nanosheets in energy storage and conversion systems, including artificial heterostructures/superlattices,<sup>11-13</sup> surface and interface engineering,<sup>14-17</sup> size/composition tuning,<sup>18</sup> phase

engineering,<sup>19</sup> heteroatom doping/substitution,<sup>20-23</sup> and vacancy engineering.<sup>24-28</sup>

Among these strategies, vacancy engineering of 2D nanosheets is one of the most straightforward and effective approaches to achieving high performance. Vacancies exist widely in 2D nanomaterials, which enables tuning the electronic and structural properties. Especially, atomic vacancies can further regulate the electronic and surface structure of materials at an atomic level, thus resulting in unprecedented electrochemical properties. On the one hand, atomic vacancies can increase the electronic conductivity of 2D nanosheets and act as additional sites in the process of charge storage.<sup>29-31</sup> On the other hand, introduction of atomic vacancies in 2D nanosheets can not only modulate electronic structures but also improve the number of effective active sites to boost catalytic activities.<sup>32-35</sup> For example, the oxygen vacancies in LiV<sub>3</sub>O<sub>8</sub> nanosheets not only improved the electrical conductivity but also enhanced the diffusion rates of lithium ions, resulting in high rate capability and stability of LiV<sub>3</sub>O<sub>8</sub> nanosheet anodes for lithium storage.<sup>36</sup> Through the introduction of sulfur vacancies, the MoS<sub>2</sub> nanosheets obtained excellent HER performance because of the increased active sites.<sup>37</sup> Compared with atomic anion vacancies, the atomic cation vacancies are less studied in this field, which may be due to the difficulty in the synthesis and characterization of cation vacancies. With the accelerating development of advanced synthetic strategies and characterization techniques, the incorporation of atomic cation vacancies within 2D nanosheets has also been extensively investigated in recent years.<sup>25,38,39</sup> For instance, Xiong et al. reported that Ti atomic vacancies in Ti<sub>0.87</sub>O<sub>2</sub> nanosheets can reduce the shuttling effect of polysulfide/polyselenide anions and promote fast transport of alkali ions, resulting in high-perf-

<sup>a</sup> Key Laboratory for Soft Chemistry and Functional Materials of Ministry Education, School of Chemistry and Chemical Engineering, Nanjing University of Science and Technology, Nanjing, 210094, China. E-mail: pan.xiong@njust.edu.cn, zhujw@njust.edu.cn

<sup>b</sup> International Center for Materials Nanoarchitectonics (WPI-MANA), National Institute for Materials Science (NIMS), Namiki 1-1, Tsukuba, Ibaraki, 305-0044, Japan. E-mail: sasaki.takayoshi@nims.go.jp

<sup>†</sup> These authors contributed equally to this work.

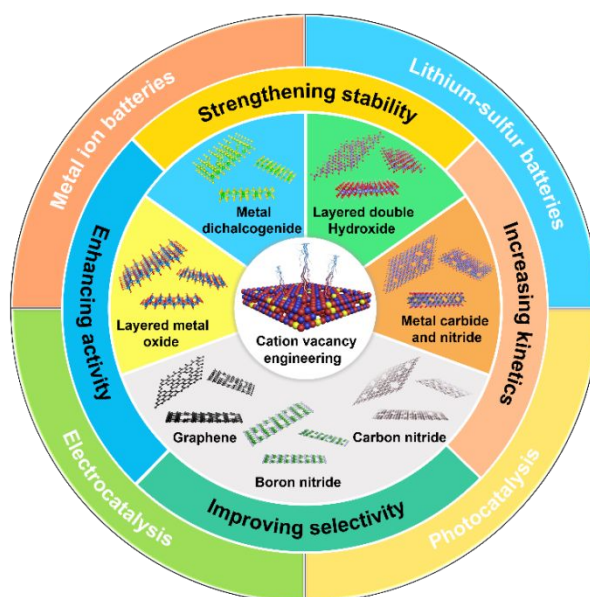


**Fig. 1 Schematic diagram of atomic cation-vacancy engineering of some typical 2D nanosheets for energy-related applications.** Schematic showing the applications of 2D cation-deficient nanosheets of LTMO nanosheets, TMD nanosheets, LDH nanosheets, MXene nanosheets, graphene, BN and CN nanosheets in metal ion batteries, lithium-sulfur batteries, electrocatalysis, and photocatalysis. The cation vacancy engineering of 2D nanosheets improves their electrochemical performance in reaction activity, selectivity, kinetics and stability.

ormance Li-S, Li-Se, and Na-Se batteries with a long-term cycling stability.<sup>40</sup> The cation vacancies in 2D nanosheets as electrode materials also play a key role in energy storage processes. Mn vacancies of 2D  $\delta$ -MnO<sub>2</sub> nanosheets provide additional ion intercalation sites for improved specific capacitances and cycling stability.<sup>41</sup> In addition, the Fe or Ni vacancies in NiFe LDHs nanosheets could increase the adsorption capacity of reaction intermediates via tuning the surface electronic structure, which resulted in a superior OER activity.<sup>42</sup> Those reports have demonstrated the recent great advances in atomic cation-vacancy engineering of 2D nanosheets for energy-related applications. A timely summary of the latest discoveries and achievements should be systematically and comprehensively conducted for future research.

In this review, we focus on recent progress in the atomic cation-vacancy engineering of 2D nanosheets for energy-related applications (Fig. 1). We introduce the synthetic strategies and characterization methods of cation vacancies in various 2D nanosheets, including layered transition metal oxide (LTMO) nanosheets, transition metal dichalcogenide (TMD) nanosheets, LDH nanosheets, MXene nanosheets, graphene, boron nitride (BN) and carbon nitride (CN) nanosheets. Then, we discuss the improved electrochemical performance of these cation-deficient 2D nanosheets for some typical energy-related systems, such as metal ion batteries, lithium-sulfur batteries, electrocatalysis and photocatalysis. Finally, we provide an outlook on current challenges and future perspectives.

## 2. Two-dimensional nanosheets with cation vacancies

Due to the fascinating and unique properties of atomic thickness, large specific surface area and excellent mechanical flexibility,<sup>43,44</sup> 2D nanosheets are promising candidates for atomic cation-vacancy engineering. So far, considerable efforts have been devoted to the preparation of various 2D cation-deficient nanosheets (Fig. 2). These synthetic strategies of cation vacancies in diverse 2D nanosheets can be roughly classified into four categories, that is, wet-chemistry, thermal annealing, ion/electron beam irradiation and selective etching (Fig. 3). Wet-chemistry method is a relatively green and safe means to directly trigger the formation of cation vacancies accompanied by the preparation of ultrathin 2D materials. Generally, the cation vacancy content introduced by this method is not arbitrarily controllable. In contrast, thermal annealing, ion/electron beam irradiation and selective etching methods are based on post-treatment of ultrathin 2D materials to induce a tunable vacancy concentration.<sup>45</sup> The cation vacancy concentration can be precisely regulated by controlling the reaction conditions, such as thermal annealing atmosphere and temperature, etchant concentration, and ion/electron beam dosage. But these synthetic methods might cause a lot of extraneous damage to the material during the preparation process.<sup>19</sup> In this section, we discuss the synthetic strategies and characterization methods of cation vacancies in diverse 2D nanosheets, including LTMO nanosheets, TMD nanosheets, LDH

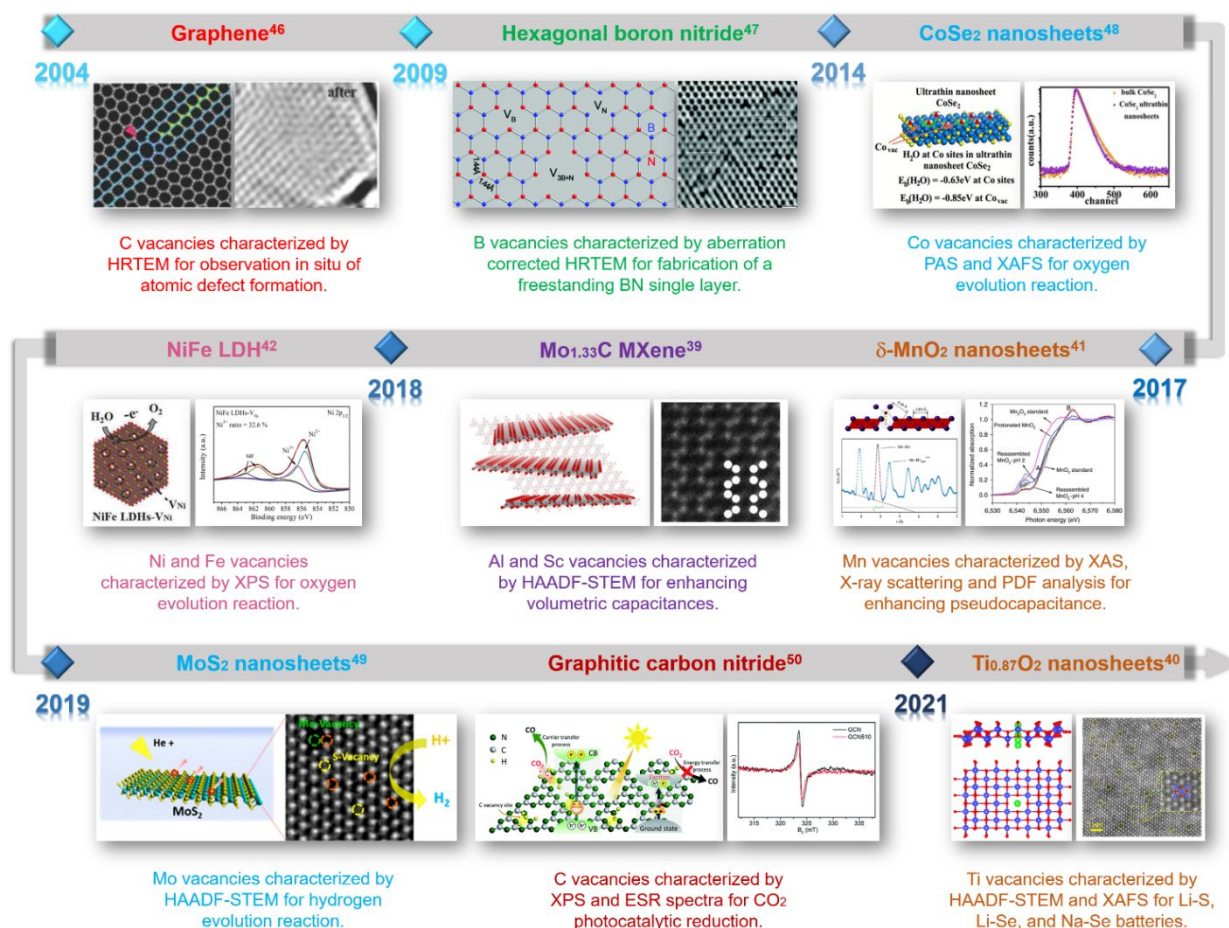


**Fig. 2 Timeline of the development of fabrication and characterization of 2D cation-deficient nanosheets.** Reproduced with permission.<sup>46</sup> Copyright 2004, Springer Nature. Reproduced with permission.<sup>47</sup> Copyright 2009, APS. Reproduced with permission.<sup>48</sup> Copyright 2014, ACS. Reproduced with permission.<sup>39,41</sup> Copyright 2017, Springer Nature. Reproduced with permission.<sup>42</sup> Copyright 2018, Wiley-VCH. Reproduced with permission.<sup>49</sup> Copyright 2019, ACS. Reproduced with permission.<sup>50</sup> Copyright 2019, RSC. Reproduced with permission.<sup>40</sup> Copyright 2021, Springer Nature.

nanosheets, MXene nanosheets, graphene, BN and CN nanosheets.

### 2.1 Layered transition metal oxide nanosheets

LTMO nanosheets are ideal platforms to study the impacts of cation vacancies within the nanosheets.<sup>41,51-53</sup> Some wet-chemistry methods have been explored to create cation vacancies within the 2D LTMO nanosheets, such as ion exchange-assisted exfoliation method and pH-treatment. The ion exchange-assisted exfoliation method can directly induce the in situ formation of cation vacancies during the delamination of layered parent crystals into 2D LTMO nanosheets.<sup>54</sup> Although the aforementioned synthesis method can be used for the preparation of ultrathin 2D cation-deficient LTMO nanosheets, the synthetic procedures are complicated and time-consuming, thus largely restricting their large-scale commercial applications.<sup>55,56</sup> For example, cation-deficient titanium oxide nanosheets,  $\text{Ti}_{1-6}\square_6\text{O}_2$ <sup>46-</sup>, where  $\square$  represents the atomic Ti vacancies, are prepared via an ion exchange-assisted exfoliation process (Fig. 4a).<sup>51,57</sup> The layered parent titanate,  $\text{K}_{0.8}\text{Ti}_{1.73}\text{Li}_{0.27}\text{O}_4$ , is first synthesized by a solid-state calcination process. In this structure,  $\text{Li}^+$  ions partially substitute  $\text{Ti}^{4+}$  sites in

the host layer, and resulting negative charge is compensated for by accommodating  $\text{K}^+$  ions into the interlayer space. Then, during an ion-exchange process, the intercalated  $\text{K}^+$  ions are exchanged by hydrated protons while the  $\text{Li}^+$  ions are extracted from the lattices, resulting in the formation of a layered protonated form with Ti atomic vacancies,  $\text{H}_{1.07}\text{Ti}_{1.73}\square_{0.27}\text{O}_4 \cdot \text{H}_2\text{O}$ . In the last step, the layered protonated titanate is reacted with a solution containing organo-ammonium ions, which induces enormous interlayer expansion as a result of the permeation of a massive volume of water. The swollen structure is collapsed by manual or mechanical shaking, generating a stable colloidal suspension of exfoliated  $\text{Ti}_{0.87}\text{O}_2$  nanosheets.<sup>58-60</sup> The obtained  $\text{Ti}_{0.87}\text{O}_2$  nanosheets are unilamellar 2D crystals with a thickness of  $\sim 1.1$  nm (Fig. 4b). The atomic Ti vacancies and their distribution on  $\text{Ti}_{0.87}\text{O}_2$  nanosheets can be directly observed in high-angle annular dark-field scanning transmission electron microscopy (HAADF-STEM) images (Figs. 4c and 4d). Furthermore, compared to those of rutile  $\text{TiO}_2$  without Ti vacancies,  $\text{Ti}_{0.87}\text{O}_2$  nanosheets show a stronger pre-edge peak in the Ti K-edge X-ray absorption near edge structure (XANES) spe-

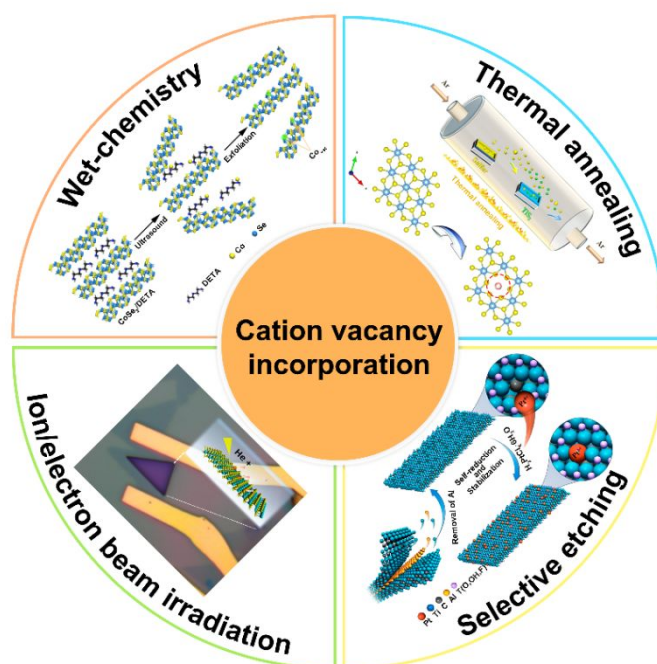


**Fig. 3 Schematic diagram of synthetic strategies of intentionally incorporating cation vacancies into 2D nanosheets.** Schematic showing the four synthetic approaches of various 2D cation-deficient nanosheets, including wet-chemistry, thermal annealing, ion/electron beam irradiation and selective etching. Reproduced with permission.<sup>48</sup> Copyright 2014, ACS. Reproduced with permission.<sup>49</sup> Copyright 2019, ACS. Reproduced with permission.<sup>61</sup> Copyright 2020, Elsevier. Reproduced with permission.<sup>62</sup> Copyright 2019, ACS.

ctra (Fig. 4e), less intense Ti K-edge extended X-ray absorption fine spectroscopy (EXAFS)  $k^3 \chi(k)$  oscillation curve (Fig. 4f), and major coordination peak in Fourier transformed (FT) curves of Ti K-edge EXAFS (Fig. 4g). All these features indicate the presence of Ti vacancies in the resulting  $\text{Ti}_{0.87}\text{O}_2$  nanosheets.

The pH-treatment is a post-processing method to ex situ introduce cation vacancies with tunable concentrations by controlling the pH value of the suspensions of 2D LTMO nanosheets. However, the obtained LTMO nanosheets normally do not remain as well-dispersed monolayers, but rather aggregate to form 3D porous nanostructures when using this method.<sup>63</sup> For instance, Mn vacancies were introduced into  $\delta$ - $\text{MnO}_2$  nanosheets via equilibrating the nanosheets at specific pH values.<sup>41</sup> This type of defect as “surface Frenkel defects” includes an in-plane Mn vacancy and a six-fold coordinated  $\text{Mn}^{3+}$  site, which was formed by the reduction of  $\text{Mn}^{4+}$  to  $\text{Mn}^{3+}$  at the  $\delta$ - $\text{MnO}_2$  surface. The content of the Mn vacancy in  $\delta$ - $\text{MnO}_2$  nanosheets could be controlled by adjusting the pH of the colloidal suspension. As the pH value decreased, the protons absorbed on the surface of  $\delta$ - $\text{MnO}_2$  nanosheets were increased. Consequently, the reduction of  $\text{Mn}^{4+}$  to  $\text{Mn}^{3+}$  was promoted, increasing the number of expelled in-plane Mn and thus more Mn vacancies.

## 2.2 Transition metal dichalcogenide nanosheets

The introduction of cation vacancies within 2D TMD nanosheets could also be achieved by in situ construction and ex situ formation.<sup>64–68</sup> The in-situ construction methods generally create cation vacancies during the synthetic processes of TMD

nanosheets. For example, Xie’s group reported the synthesis of  $\text{CoSe}_2$  nanosheets with Co vacancies by chemical exfoliation of layered  $\text{CoSe}_2$ /diethylenetriamine ( $\text{CoSe}_2$ /DETA) intermediates (Fig. 5a).<sup>48</sup> Since the EDTA is coordinately bonded to Co atoms, it could drag Co atoms out of the  $\text{CoSe}_2$  lattices during the ultrasonic exfoliation, thus forming Co vacancies on the  $\text{CoSe}_2$  nanosheets. Both the tree lifetime components of positron annihilation spectroscopy (PAS) (Fig. 5b) and the peak intensities of the nearest Co-Se coordination in FT curves of Co K-edge EXAFS (Fig. 5c) indicated that Co vacancies were successfully generated in  $\text{CoSe}_2$  nanosheets. The cation vacancies could also be in situ constructed in TMD nanosheets during a chemical vapor deposition (CVD) process. Gao et al. prepared  $\text{MoSe}_2$  nanosheets with both Mo and Se vacancies by adjusting the growth temperatures of CVD (Figs. 5d and 5e).<sup>69</sup> Besides, more Mo and Se vacancies were formed in the nanosheets compared with the microparticles and nanoplates (Figs. 5f and 5g).

Compared with in situ construction, the ex situ formation is a post-synthesis method for the intentional generation of cation vacancies within TMD nanosheets, which has been realized by several techniques, including ion-beam irradiation,<sup>49,70</sup> high-temperature annealing<sup>61</sup> and acid etching.<sup>71</sup> Note that these synthetic methods can induce a tunable vacancy by precisely controlling the reaction conditions, but the rigid preparation conditions could destroy the structure of TMD nanosheets.<sup>18,72</sup> A focused  $\text{Ga}^+$  ion beam irradiation method (Fig. 5h) had been used to engineer cation vacancies in

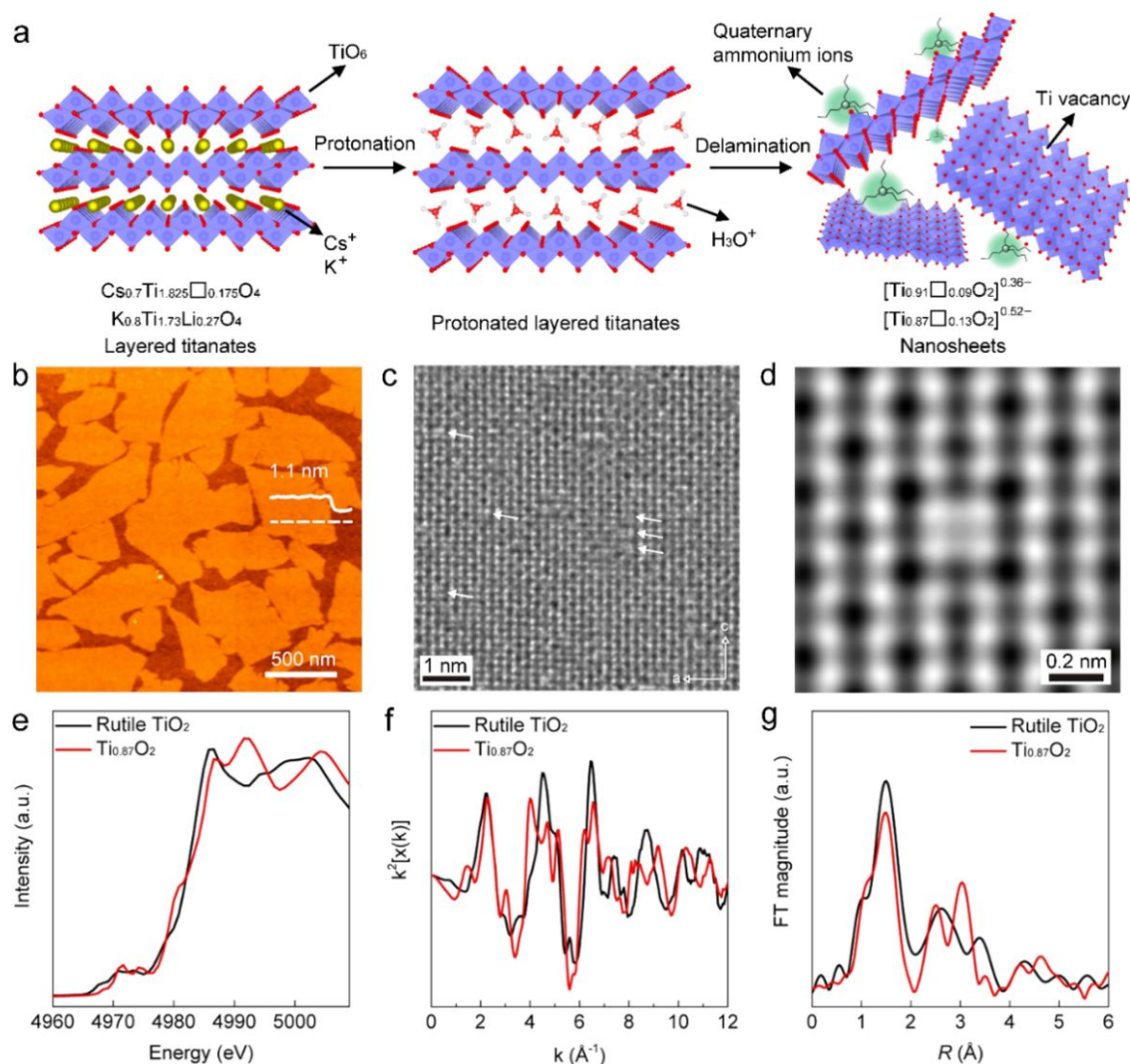


**Fig. 4 Formation of cation vacancies in LTMO nanosheets.** (a) Schematic illustration of exfoliation of the layered titanate into 2D  $\text{Ti}_{1-x}\text{O}_2^{46-}$  nanosheets. (b) AFM image, (c) high-resolution TEM image and (d) corresponding expanded image taken in the [010] direction of  $\text{Ti}_{0.87}\text{O}_2$  nanosheets. Reproduced with permission.<sup>58</sup> Copyright 2013, Springer Nature. (e) The Ti K-edge XANES spectra, (f) EXAFS  $k^3\chi(k)$  oscillation curves and (g) corresponding FT curves of rutile  $\text{TiO}_2$  and  $\text{Ti}_{0.87}\text{O}_2$  nanosheet. Reproduced with permission.<sup>40</sup> Copyright 2021, Springer Nature.

$\text{WS}_2$  and  $\text{MoS}_2$  flakes (Figs. 5i and 5j).<sup>73</sup> Similarly, through  $\text{He}^+$  ion beam irradiation, Yang et al. introduced Mo vacancies in the basal plane of  $\text{MoS}_2$  nanosheet.<sup>49</sup> Besides, the vacancy concentration could be controlled by changing the dosages of  $\text{He}^+$  ions (Fig. 5k). The generation of vacancies within the nanosheets induced deviation of atomic planes from their equilibrium positions (Fig. 5l). As a result, the variation of interatomic Mo-Mo distance was obviously detected near the vacancy sites (Fig. 5m).

### 2.3. Layered double hydroxide nanosheets

Introduction of cation vacancies within 2D LDH nanosheets has been widely examined as an effective approach to improving their electrochemical properties.<sup>74,75</sup> Wang and co-workers explored a water-plasma-enabled exfoliation for the formation of multiple

vacancies (including O, Co, and Fe vacancies) in the CoFe-LDH nanosheets (Fig. 6a).<sup>76</sup> The water plasma can destroy the electrostatic interactions between host layers and interlayer ions, which leads to the efficient exfoliation of CoFe-LDH nanosheets and the introduction of abundant vacancies within the exfoliated nanosheets. Later, they reported the synthesis of CoFe-LDHs nanosheets with Co and Fe cation vacancies through a dry exfoliation method, Ar plasma etching-assisted exfoliation.<sup>77</sup> However, it should be noted that the plasma-assisted exfoliation method could remarkably destroy the ionic bonds between cations and oxygen in the host layers, tending to the introduction of multiple vacancies.<sup>78</sup>

In contrast to the above multiple vacancies, the selective formation of cation vacancies within LDH nanosheets is more attractive. Wang et al. reported NiFe-LDHs nanosheets with selective Fe or Ni vacancies via a strong alkaline etching strategy (Fig. 6b).<sup>42</sup> A-

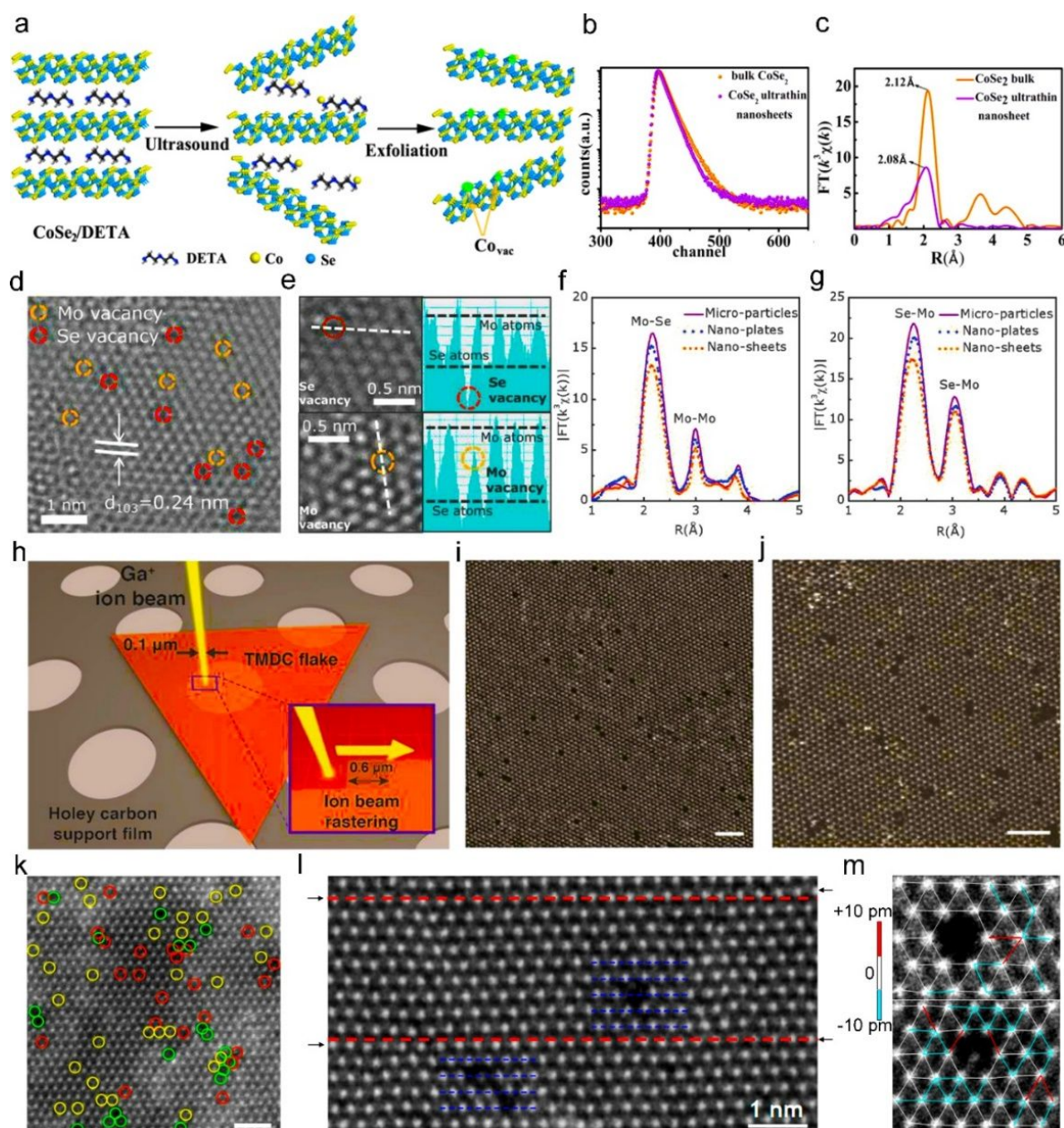


**Fig. 5 Introduction of cation vacancies within TMD nanosheets.** (a) Schematic illustration of the formation of Co vacancies in CoSe<sub>2</sub> nanosheets. (b) positron lifetime spectrum and (c) FT curves of Co K-edge EXAFS of CoSe<sub>2</sub> nanosheets and bulk CoSe<sub>2</sub>. Reproduced with permission.<sup>48</sup> Copyright 2014, ACS. (d) atomic HRTEM image, and (e) observations of Mo and Se vacancies. (f) Mo K-edge and (g) Se K-edge FT curves for MoSe<sub>2</sub> nanoplates, nanosheets, and microparticles. Reproduced with permission.<sup>69</sup> Copyright 2018, Wiley-VCH. (h) Graphic of irradiation mechanism on a TMD flake using a Ca<sup>+</sup> ion beam. HAADF images of (i) WS<sub>2</sub> and (j) MoS<sub>2</sub> flakes after FIB irradiation. Reproduced with permission.<sup>73</sup> Copyright 2019, Wiley-VCH. (k) HAADF-STEM images and (l-m) observations of local strain in MoS<sub>2</sub> nanosheets with a vacancy concentration of  $5.7 \times 10^{14} \text{ cm}^{-2}$ . Reproduced with permission.<sup>49</sup> Copyright 2019, ACS.

amphoteric Al<sup>3+</sup> and Zn<sup>2+</sup> cations could be etched in strong alkaline solutions for the creation of M<sup>3+</sup> and M<sup>2+</sup> vacancies, respectively. As a result, two kinds of precursors, NiFeAl-LDHs and NiZnFe-LDHs, were designed for the precise introduction of Fe<sup>3+</sup> and Ni<sup>2+</sup> vacancies in the resulting NiFe-LDHs, respectively. Similarly, Ni<sup>2+</sup>, Fe<sup>3+</sup>, and Ni<sup>2+</sup>/Fe<sup>3+</sup> vacancies were selectively introduced into the NiFe-LDH nanosheets by alkaline etching of Zn<sup>2+</sup>, Al<sup>3+</sup>, and Zn<sup>2+</sup>/Al<sup>3+</sup>-doped NiFe-LDHs, respectively.<sup>79</sup> A newly formed Raman signal

corresponding to cation vacancies was clearly observed for all cation-deficient NiFe-LDH samples (Fig. 6c). Moreover, FT-EXAFS curves at Fe K-edge showed that the introduced Ni<sup>2+</sup> vacancies can lower the Ni-M and Fe-M coordination numbers (Figs. 6d and 6e). While the introduction of Fe<sup>3+</sup> vacancies mainly decreased the Ni-M coordination number (Fig. 6e).

#### 2.4 Transition metal carbide and nitride nanosheets

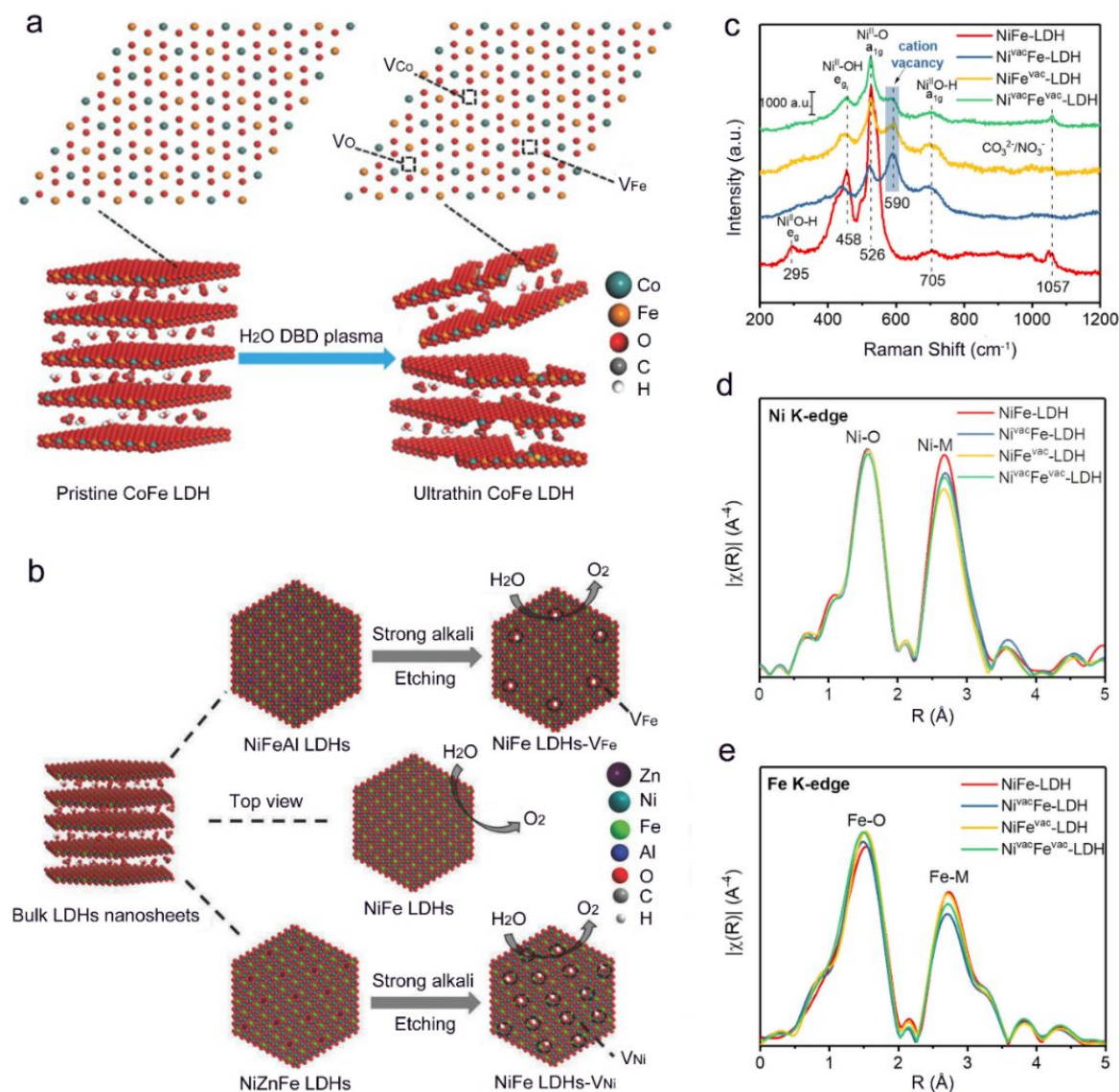


**Fig. 6 Introduction of cation vacancies into LDH nanosheets.** (a) Schematic illustration of the water-plasma-enabled exfoliation of CoFe-LDH nanosheets. Reproduced with permission.<sup>76</sup> Copyright 2017, Wiley-VCH. (b) Schematic illustration of the synthesis of NiFe-LDH nanosheets with the selective cation vacancies by strong alkali etching strategies. Reproduced with permission.<sup>42</sup> Copyright 2018, Wiley-VCH. Raman spectra (c), FT-EXAFS curves at (d) Fe K-edge, and (e) Ni K-edge for NiFe-LDH nanosheets with cation vacancies and pristine NiFe-LDH nanosheets. Reproduced with permission.<sup>79</sup> Copyright 2021, Wiley-VCH

The MXene nanosheets are generally obtained by selective etching assisted-exfoliation of layered MAX phases.<sup>80-82</sup> Sang et al. observed that Ti vacancies were formed on Ti<sub>3</sub>C<sub>2</sub>T<sub>x</sub> nanosheets during a hydrofluoric acid (HF) etching assisted-exfoliation process (Fig. 7a).<sup>83</sup> Excessive HF removed Al layers and further destroyed the interlayer Ti-C covalent interactions to form Ti vacancies. Furthermore, the average concentrations of Ti vacancies could be controlled by the HF concentrations (Fig. 7b). Chen et al. also found that Ti vacancies in disordered single sites or clusters form on Ti<sub>3-x</sub>C<sub>2</sub>T<sub>y</sub> nanosheets prepared through the selective etching assisted-exfoliation under mild HF conditions.<sup>62</sup> However, the above HF etching assisted-exfoliation process usually generated disordered vacancies and random vacancy clusters. The introduction of ordered vacancies

within the MXene nanosheets is a great challenge.<sup>62,84,85</sup> In this regard, Rosen et al. realized the introduction of ordered divacancies in Mo<sub>1.33</sub>C nanosheets by a HF selective etching strategy (Fig. 7c).<sup>39</sup> In pristine (Mo<sub>2/3</sub>Sc<sub>1/3</sub>)<sub>2</sub>AlC, HF completely etched the amphoteric Al and Sc atoms but maintained the Mo<sub>1.33</sub>C framework. The obtained Mo<sub>1.33</sub>C nanosheets displayed hexagonal-based crystals with ordered divacancies (Figs. 7d and 7e). Based on this divacancy concept, Persson's group achieved the synthesis of Mo<sub>1.33</sub>C nanosheets with highly uniform and ordered bivacancies via controlling the HF concentration and etching time (Fig. 7f).<sup>38</sup> Apparent vacancy clusters were observed at a high HF concentration (Figs. 7g and 7h). In contrast with high concentration HF etching, mild HF etching produced the Mo<sub>1.33</sub>C nanosheets with highly ordered bivacancies

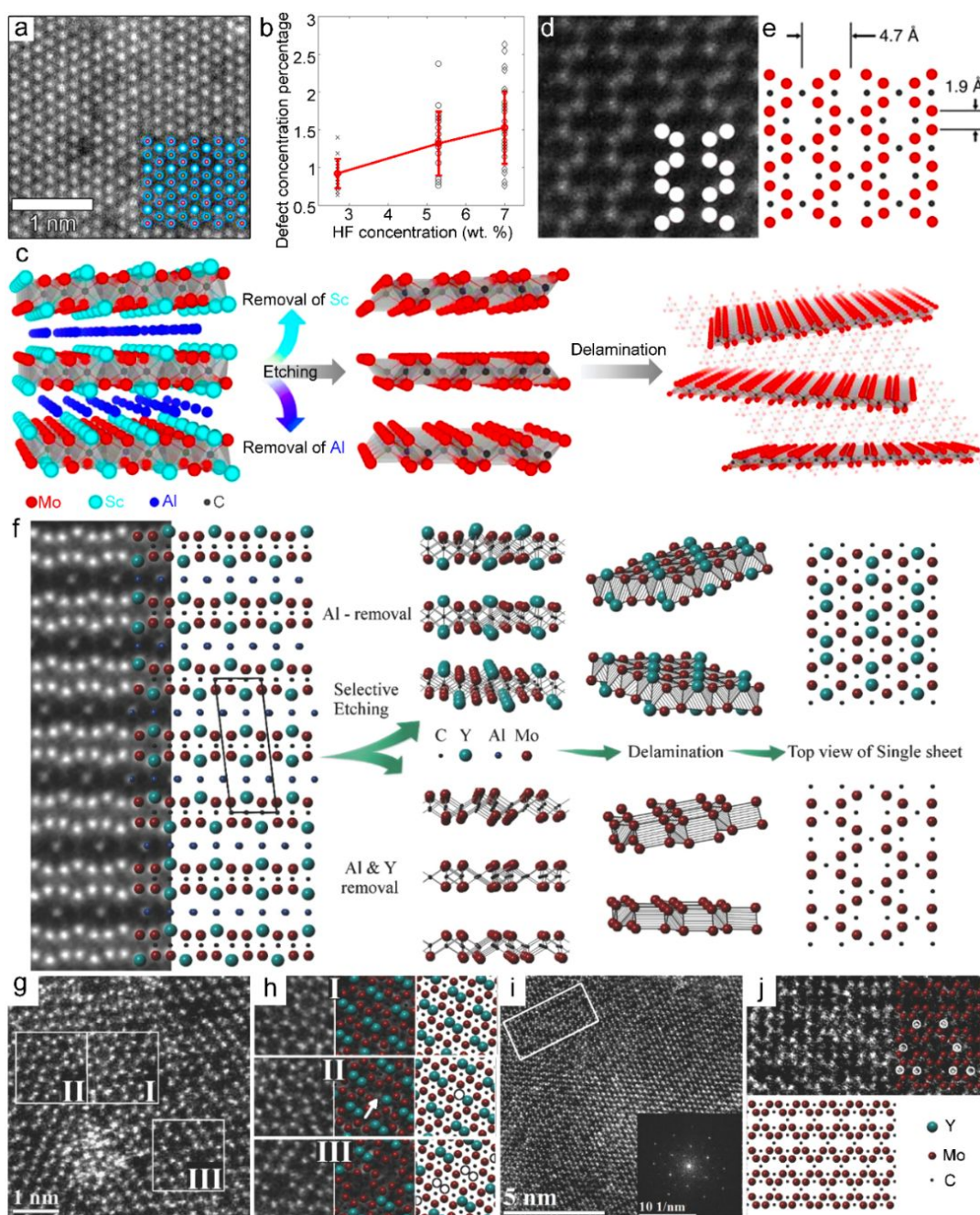


**Fig. 7 Identification of cation vacancies in MXene nanosheets.** (a) HAADF-STEM image of  $\text{Ti}_3\text{C}_2\text{T}_x$  showing the Ti atom hexagonal lattice aligned along the c axis. (b) Scatter plot of cation vacancy concentration from images acquired from samples produced using different HF concentrations. Reproduced with permission.<sup>83</sup> Copyright 2016, ACS. (c) Schematic of  $(\text{Mo}_{2/3}\text{Sc}_{1/3})_2\text{AlC}$  before etching, after etching and after delamination. (d) Atomically resolved image of  $\text{Mo}_{1.33}\text{C}$  nanosheets with overlaid schematic atomic structure. (e) Ideal atomic structure of  $\text{Mo}_{1.33}\text{C}$  nanosheets from theoretically simulated parent MAX phase. Reproduced with permission.<sup>39</sup> Copyright 2017, Springer Nature. (f) Left: STEM image of  $(\text{Mo}_{2/3}\text{Y}_{1/3})_2\text{AlC}$  with corresponding structure model. Middle: two different structures are obtained depending on etching protocol. Right: top view of corresponding structures. (g) STEM image of  $(\text{Mo}_{2/3}\text{Y}_{(1-x)/3})_2\text{C}$  nanosheet. (h) Enlarged region indicated in panel (g). (i) Atomically resolved image of the vacancy ordered  $\text{Mo}_{1.33}\text{C}$  nanosheets. (j) Magnified view of the atomic structure of (i) and top view of corresponding structures. Reproduced with permission.<sup>38</sup> Copyright 2018, Wiley-VCH.

ies (Figs. 7i and 7j). In addition to the traditional HF etching, Luo et al. introduced Ti cation vacancies into  $\text{Ti}_3\text{C}_2$  MXene nanosheets by an  $\text{NH}_3$ -etching pyrolysis approach.<sup>86</sup> During the

$\text{NH}_3$ -assisted annealing process, partial Ti atoms would be removed through the formation of volatile titanium species.<sup>87</sup>

### 2.5 Graphene, boron nitride and carbon nitride nanosheets

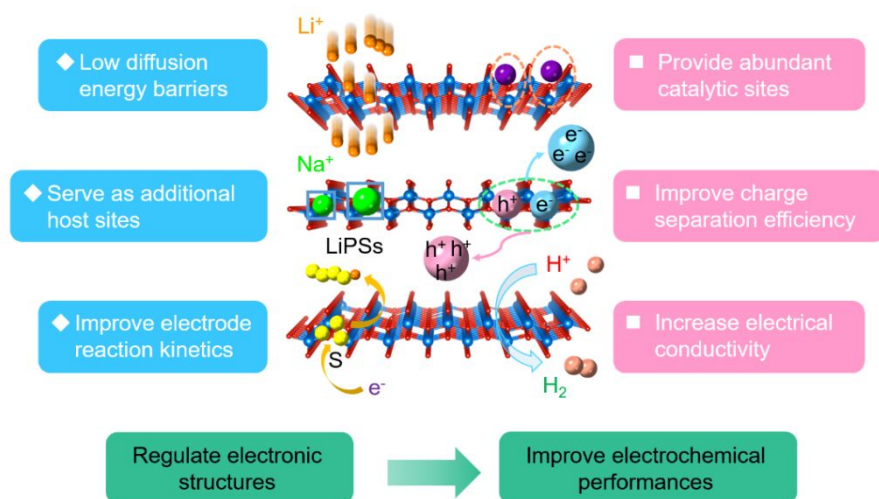


**Fig. 8 The regulation of electronic structures of 2D cation-deficient nanosheets for improving electrochemical performances.** Schematic illustrating the regulation of electronic structures of 2D cation-deficient nanosheets for electrochemical energy storage, including low diffusion energy barriers, serve as additional host sites and improve electrode reaction kinetics. The regulation of electronic structures of 2D cation-deficient nanosheets for electro/photocatalytic reactions, including provide abundant catalytic sites, improve charge separation efficiency and increase electrical conductivity.

In addition to the above 2D nanosheets, generation of cation vacancies within graphene, BN and graphitic carbon nitride (GCN) nanosheets has been explored. Among various synthetic methods of graphene oxides, the most common way is the Hummers method, which involves a strong oxidation process.<sup>88-90</sup> This may lead to the removal of carbon atoms from the lattices, resulting in the formation of carbon vacancies in reduced graphene oxide or graphene nanosheets.<sup>91</sup> Hence, a monovacancy containing a 5-element ring and a 9-element ring was observed in the graphene lattice.<sup>92</sup> In addition to the monovacancy, divacancy and trivacancy have been introduced in graphene by electron beam irradiation.

Similar to graphene, BN nanosheets possess an atomically thin 2D structure with alternating B and N atoms. Therefore, atomic B vacancies in BN nanosheets could also be created by using controlled energetic electron irradiation.<sup>47</sup> GCN nanosheet is also a graphene-like 2D structure with strong covalent C-N bonds rather than C-C bonds.<sup>93</sup> Recently, Shen et al. reported a GCN nanosheet with C vacancies (GCN-Vc) through a high temperature treatment under an  $\text{NH}_3$  atmosphere.<sup>50</sup> These C vacancies were introduced due to the loss of C atoms via  $\text{NH}_3$  etching. Note that the conjugated aromatic rings of GCN nanosheet might suffer slight destruction during selective etching.<sup>94</sup> Different from the high temperature treatment under certain atmospheres, Guan's group reported the introduction of C vacancies into GCN nanosheets via a mild chemical oxidation etching with  $\text{H}_2\text{SO}_4$ .<sup>95</sup>

### 3. 2D cation-deficient nanosheets for energy-related performances

The ultimate goal of rational 2D cation-deficient material design is to improve electrochemical performance as much as possible for certain applications. Deliberately incorporated cation

vacancies endow them with abundant advantageous characteristics on electrochemical performances including enhanced electrical conductivity, lower energy barrier for ion diffusion, extra sites for charge storage, etc. In this section, we review the recent progress on improving electrochemical energy storage and conversion performances of these 2D materials through the introduction of cation vacancies.

#### 3.1 Cation vacancies for tuning the electronic structures of 2D nanosheets

The electrochemical performances of 2D cation-deficient nanosheets are usually strongly associated with their electronic structure (Fig. 8). In general, vacancy engineering via introducing cation vacancies is believed to be one of the most efficient strategies to regulate the electronic structure of materials, thus resulting in unprecedented electrochemical properties. On the one hand, in the process of electrochemical energy storage, cation vacancies can lower the diffusion energy barriers, thus promoting the proton or alkali cation intercalation/deintercalation process. Besides, cation vacancies also serve as additional host sites for alkali cation intercalation to provide a much higher charge storage capacity. The incorporation of cation vacancies is favorable to the charge transfer process, which improves the electrode reaction kinetics. For example, Gao and co-workers reported that the Mn vacancies present in 2D d- $\text{MnO}_2$  nanosheets can change their electronic structure, and the introduction of Mn vacancies was confirmed to enhance the charge transfer process.<sup>41</sup> This could further results in improved rate capability. On the other hand, cation-vacancy engineering of 2D nanosheets not only provides abundant catalytic sites but also improves charge separation efficiency for catalytic reaction processes. In addition, the electrical conductivity of the catalyst can be increased through the introduction of cation vacancies. Undoubtedly, these alterations to the electronic structure of catalysts are very bene-

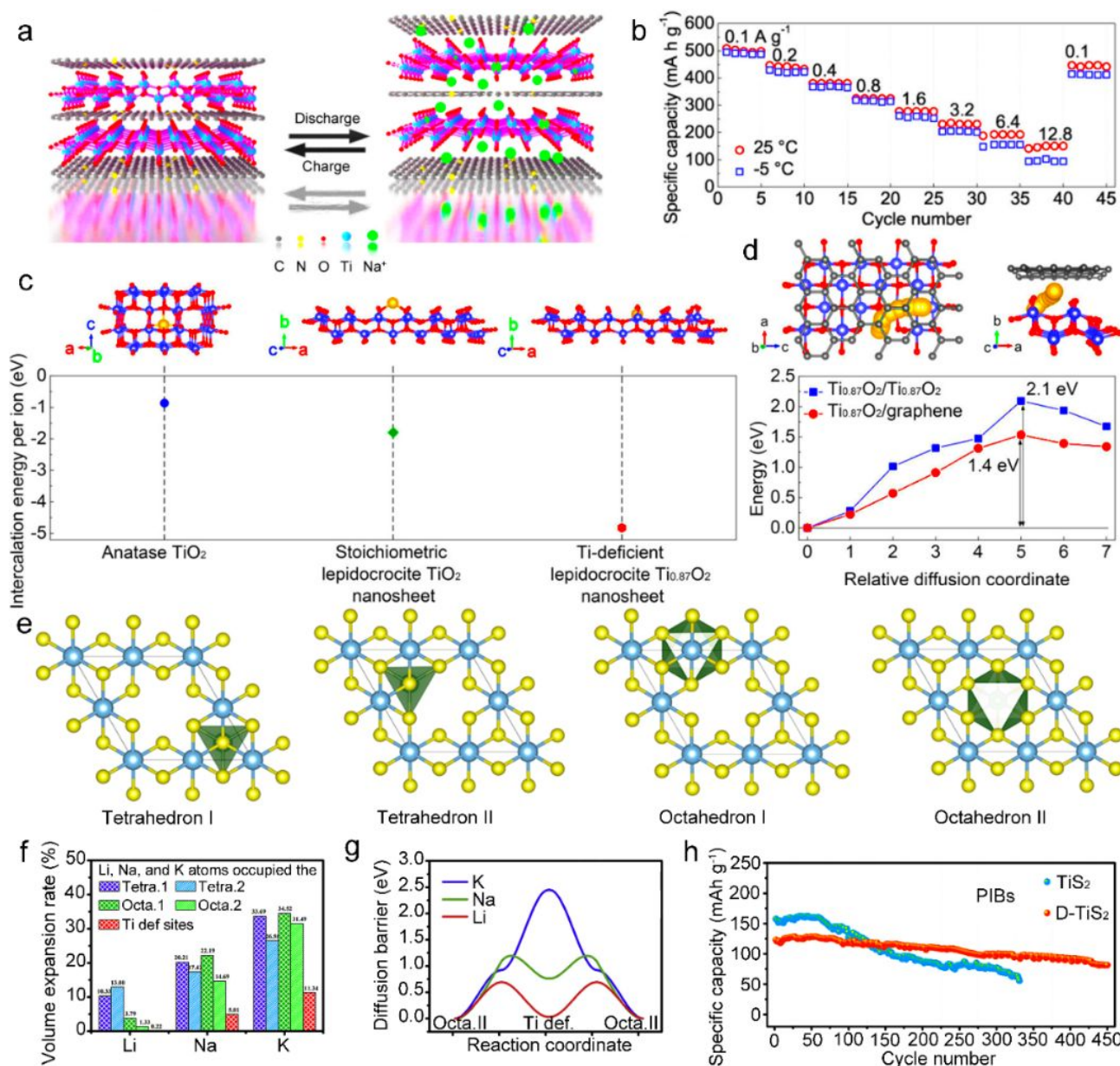


**Fig. 9 Cation-vacancy engineering of 2D nanosheets for metal ion batteries.** (a) Schematic of Na ion intercalation mechanism in the  $\text{Ti}_{0.87}\text{O}_2/\text{graphene}$  superlattice. (b) Capacity retentions at 25 and  $-5^\circ\text{C}$  at different current densities. (c) Intercalation energies for Na ions in anatase  $\text{TiO}_2$ , stoichiometric lepidocrocite-type  $\text{TiO}_2$  nanosheet, and Ti-deficient lepidocrocite-type  $\text{Ti}_{0.87}\text{O}_2$  nanosheet. (d) Effects of  $\text{Ti}_{0.87}\text{O}_2/\text{graphene}$  superlattice structure for Na diffusion. Reproduced with permission.<sup>12</sup> Copyright 2018, ACS. (e) Possible intercalation sites in Ti-defected  $\text{TiS}_2$  structure during metal ion intercalation processes. (f) Volume expansions and (g) diffusion barriers for Li, Na, and K ions in different sites. (h) Cycling performance of  $\text{TiS}_2$  and D- $\text{TiS}_2$  at a current density of  $50\text{ mA g}^{-1}$  for PIBs. Reproduced with permission.<sup>61</sup> Copyright 2020, Elsevier.

ficial for increasing their catalytic activity.<sup>96,97</sup> Xia et al. reported that intentional cation vacancy incorporation can not only result in an increased electrical conductivity but also produce more catalytic sites in  $\text{MoSe}_2$  nanosheets.<sup>70</sup> This leads to a low overpotential and Tafel slope, ensuring an excellent electrocatalytic capacity in the HER process.

### 3.2 2D cation-deficient nanosheets for energy-related applications

Considerable efforts have been devoted to the preparation of diverse 2D cation-deficient nanosheets to improve their

electrochemical performances. Herein, we summarize the recent progress on electrochemical energy storage and conversion technologies of these materials for some typical energy-related systems, such as metal ion batteries, lithium-sulfur batteries, electrocatalysis and photocatalysis.

#### 3.2.1 Metal ion batteries

Metal ion batteries such as sodium-ion batteries (SIBs), potassium-ion batteries (PIBs) and zinc-ion batteries (ZIBs) have been considered promising alternatives to conventional lithium-ion batte-

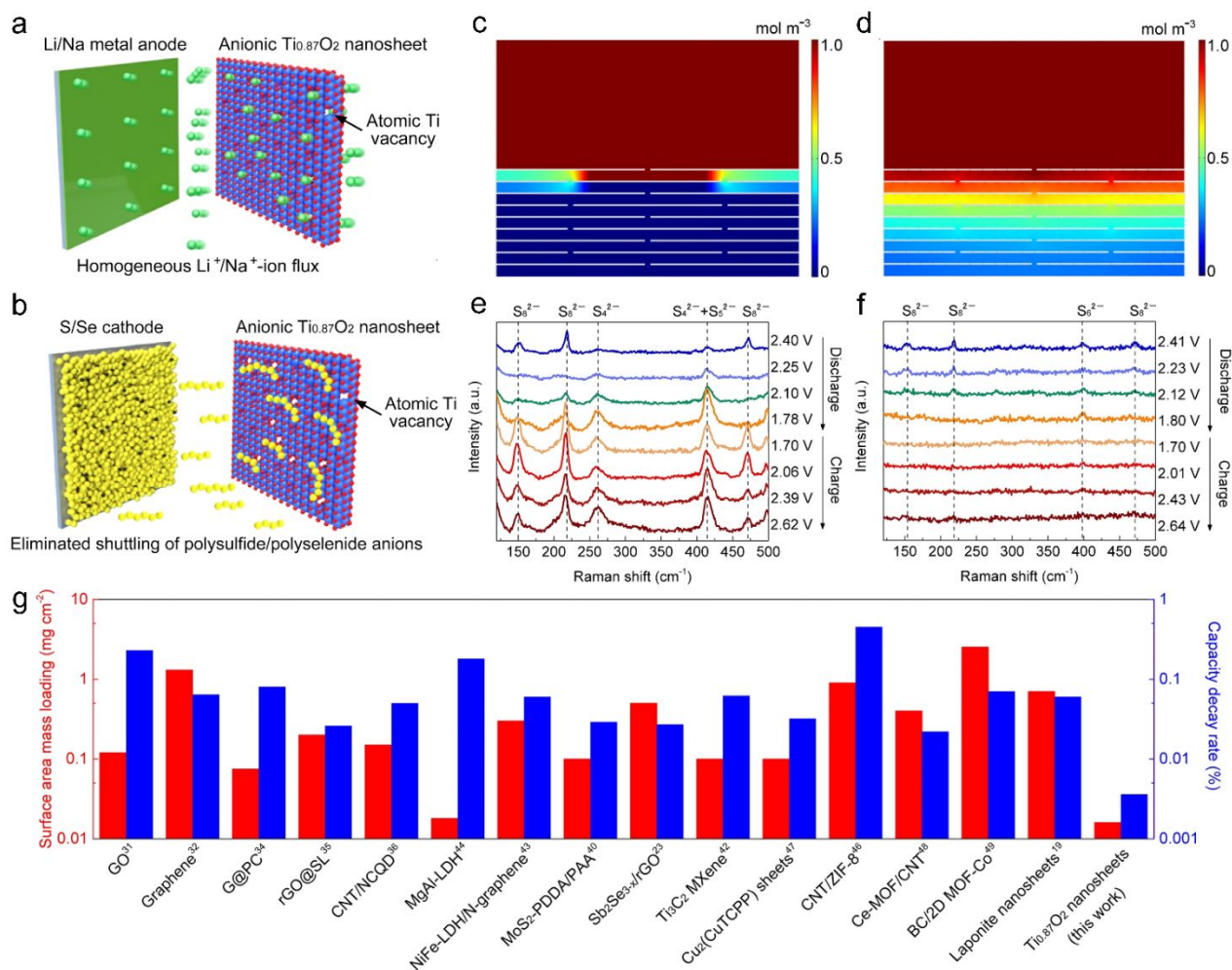


**Fig. 10** Cation-vacancy engineering of 2D nanosheets for lithium-sulfur batteries. 2D negatively charged  $\text{Ti}_{0.87}\text{O}_2$  nanosheets with Ti vacancies provide electrostatic interaction with (a)  $\text{Li}^+$  ions and (b) PS anions, resulting in homogeneous distribution of  $\text{Li}^+$ -ion flux and effective suppression of PS shuttling, respectively. The distribution of  $\text{Li}^+$  ions passing restacked nanosheets (c) with and (d) without Ti vacancies. Ex situ Raman spectra of (e)  $\text{Ti}_{0.87}\text{O}_2/\text{PP}$  and (f) PP separators retrieved from Li-S cells during the discharge and charge processes. (g) Comparison of surface area mass loading and cycling performance for  $\text{Ti}_{0.87}\text{O}_2$  nanosheets and some other reported materials. Reproduced with permission.<sup>40</sup> Copyright 2021, Springer Nature.

ries (LIBs) due to the abundance of sodium and potassium resources.<sup>98-100</sup> However, the development of suitable electrode materials with a robust storage capability of large  $\text{Na}^+$  and  $\text{K}^+$  ions is a challenge. Besides, divalent  $\text{Zn}^{2+}$  ions usually exhibit strong electrostatic interactions with the host materials, which can lead to slow  $\text{Zn}^{2+}$  diffusion and thus greatly diminish reversible capacity.<sup>101</sup> One of the most effective methods to increase the charge-storage capability of the electrode materials is introduction of cation vacancies as additional ion storage sites.

Xiong et al. explored a nanosheet superlattice composite as an anode material for SIBs, which was composed of 2D  $\text{Ti}_{0.87}\text{O}_2$  nanosheets with Ti vacancies and graphene nanosheets. The influences of Ti vacancies on sodium ion storage were systematically examined.<sup>12</sup> During the charge and discharge processes,  $\text{Na}^+$  ions are reversibly inserted into both the Ti vacancies and interlayer galleries of superlattices without a change in fundamental structure (Fig. 9a).

Consequently, a superior low-temperature rate capability was achieved (Fig. 9b). One of the main reasons for the excellent SIB performance could be attributed to favorable  $\text{Na}^+$  ion intercalation within the defective nanosheets (Fig. 9c). In addition, the superlattice structure contributed to ultrafast diffusion dynamics of  $\text{Na}^+$  ions (Fig. 9d). Similarly, Zhang and co-workers developed an ultrathin  $\text{MoS}_2$  nanosheet with Mo vacancies, which not only provides additional storage sites to vastly accelerate the charge transport but also enhances  $\text{Na}^+$  ion interaction by influencing the electronic configuration of the host material.<sup>71</sup> Therefore, an excellent specific capacity and high cycle stability were achieved by using the Mo-deficient  $\text{MoS}_2$  nanosheet anodes for SIBs.

Recently, Liu et al. investigated the possible alkali-metal (Li/Na/K) ion intercalation processes on  $\text{TiS}_2$  nanosheets with Ti vacancies (Fig. 9e).<sup>61</sup> They found that alkali metal ions insertion into the Ti vacancy sites showed the smallest volume expansion rate com-

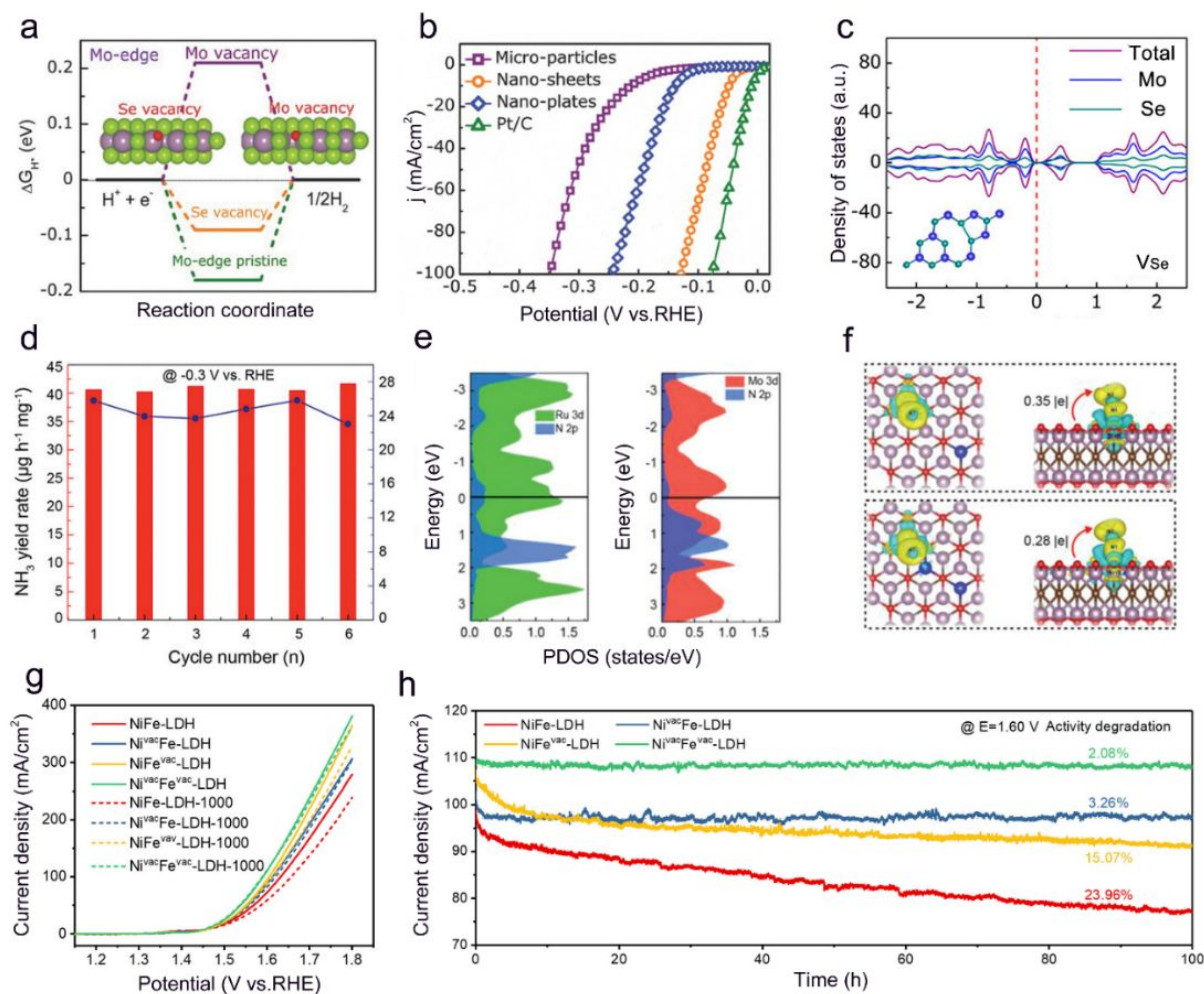


**Fig. 11 Cation-vacancy engineering of 2D nanosheets for electrocatalytic applications.** (a) The calculated HER free energy results in the case of Mo edge with Mo and Se vacancies. (b) LSV curves of different nanostructures of  $\text{MoSe}_2$  with Mo vacancies and Pt/C for HER. Reproduced with permission.<sup>69</sup> Copyright 2018, Wiley-VCH. (c) Density of states (DOS) of Mo vacancy in  $\text{MoSe}_2$  unit cell. Reproduced with permission.<sup>70</sup> Copyright 2018, ACS. (d)  $\text{NH}_3$  yield rates and Faradaic efficiencies of the  $\text{Ru-Mo}_2\text{CT}_x$  with consecutive recycling electrolysis. (e) The projected density of states (PDOS) for the N atoms bonded to Ru atoms and Mo atoms of  $\text{Ru-Mo}_2\text{CT}_x$ . (f) The charge density differences calculations of  $\text{N}_2$  bonded to Ru atoms and Mo atoms of  $\text{Ru-Mo}_2\text{CT}_x$ . Reproduced with permission.<sup>109</sup> Copyright 2020, Wiley-VCH. (j) LSV curves and (k) Chronoamperometry data of different types of cation-vacancy NiFe LDH nanosheets for OER. Reproduced with permission.<sup>79</sup> Copyright 2021, Wiley-VCH.

pared with the other intercalation processes (Fig. 9f). Different from  $\text{Li}^+$  and  $\text{Na}^+$  ions,  $\text{K}^+$  ions cannot occupy the Ti vacancy sites due to a high diffusion barrier (Fig. 9g). As a result, a superior cycle performance was achieved for the Ti-deficient  $\text{TiS}_2$  nanosheets as anodes for PIBs, outperforming the  $\text{TiS}_2$  counterparts without Ti vacancies (Fig. 9h).

In addition to the above alkali-metal ion batteries (LIBs/SIBs/PIBs), multivalent ion batteries such as ZIBs have remarkable electrochemical performance for the storage of metal ions through the introduction of cation vacancies. Pioneering work exploring the Zn ion energy storage of H-vacancy-enriched CoNi LDH demonstrated that H vacancies can provide additional intercalation sites for cations.<sup>102</sup> The partial occupancy of H vacancies by Zn ions could effectively increase electrical conductivity, accelerate diffusion kinetics and enhance the storage capacity. Therefore, a high specific

capacity was achieved by using the H-deficient CoNi LDH nanosheet cathodes for high-performance mild Zn ion batteries.

### 3.2.2 Lithium-sulfur batteries

Lithium-sulfur batteries are an attractive next-generation energy storage system due to their high theoretical energy densities and low cost.<sup>103-105</sup> However, some major challenges associated with both S cathodes and Li anodes have severely impeded their commercial applications, such as the detrimental shuttle effect of soluble polysulfide (PS) intermediates and the formation of Li dendrites.<sup>106-108</sup> All these obstacles are related to the uneven migration of PS anions and  $\text{Li}^+$  cations. Thus, a desirable approach should focus on the regulation of migration of both PS anions and  $\text{Li}^+$  cations simultaneously.

In this regard, Xiong et al. designed a polypropylene (PP) separator coated with  $\text{Ti}_{0.87}\text{O}_2$  nanosheets with Ti atomic vacancies t-

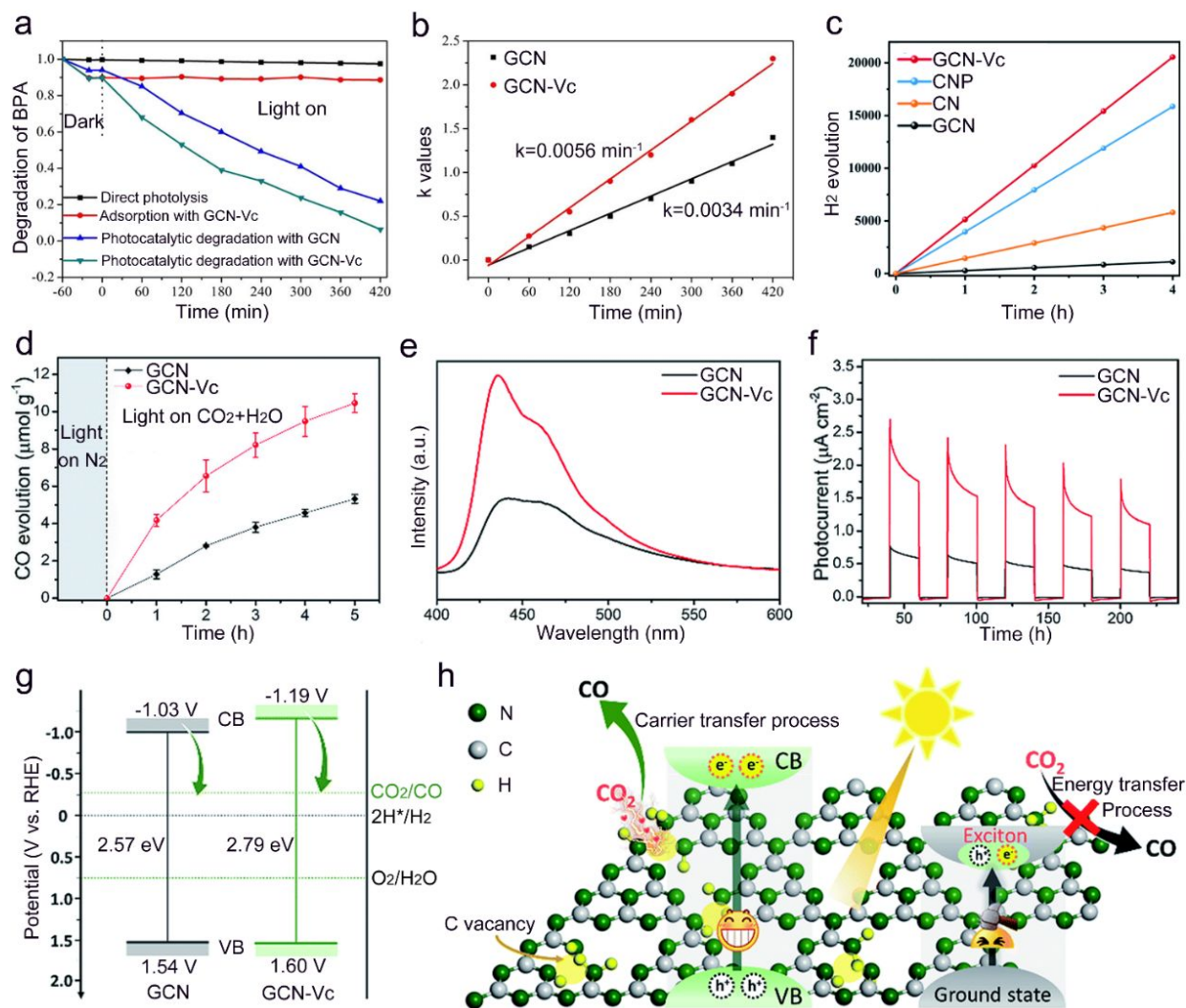


**Fig. 12 Cation-vacancy engineering of 2D nanosheets for photocatalytic applications.** (a) Degradation of bisphenol A (BPA) (b) and corresponding  $k$  values with GCN-Vc and GCN under visible light. Reproduced with permission.<sup>24</sup> Copyright 2018, ACS. (c) The photocatalytic  $H_2$  evolution of GCN-Vc, GCN and other reference samples. Reproduced with permission.<sup>95</sup> Copyright 2021, RSC. (d) The photocatalytic CO evolution, (e) photoluminescence (PL) spectra, and (f) transient photocurrent response of GCN-Vc and GCN. (g) Band position schematic of GCN-Vc and GCN. (h) Schematic representation of the activated  $CO_2$  photoreduction activity on GCN-Vc. Reproduced with permission.<sup>50</sup> Copyright 2019, RSC.

o tackle these issues.<sup>40</sup> The advantage of Ti atomic vacancies of  $Ti_{0.87}O_2$  nanosheets manifest when acted as a selective ionic sieve, can simultaneously regulate the migration of  $Li^+$  cations and PS anions at an atomic scale. On the one hand, Ti vacancies endow the  $Ti_{0.87}O_2$  nanosheets with negative charges, leading to a strong electrostatic interaction for promoting the uniform distribution of  $Li^+$  ions and then a reduced growth of Li dendrite (Fig. 10a). On the other hand,  $Ti_{0.87}O_2$  nanosheets show a strong electrostatic repulsion for effective mitigation of PS anion shuttling (Fig. 10b). Moreover, Ti atomic vacancies act as sub-nanometer pores, not only providing fast diffusion pathways of small  $Li^+$  ions but also selectively excluding the migration of large PS anions, which results in the uniform distribution of  $Li^+$  ions (Figs. 10c and 10d) and suppression of PS shuttling (Figs. 10e and 10f). Therefore,  $Ti_{0.87}O_2$  nanosheets with Ti atomic vacancies exhibited a better cycling performance as functionalized separators

for Li-S batteries compared with some reported materials (Fig. 10g). In addition, the same excellent performance can be obtained in Li-Se and Na-Se batteries by using the PP separator coated with  $Ti_{0.87}O_2$  nanosheets.

Recently, Zhang's group reported a Zn defective  $Zn_{0.875}Co_2O_4$  nanosheets applied to the PP separator for lithium-sulfur batteries.<sup>106</sup> Through introducing Zn vacancies, the  $Zn_{0.875}Co_2O_4$  nanosheets can act as a PS-blocking layer to anchor PS molecules by strong chemical adsorption, which shows a superior effect on suppressing the PS shuttle and improving reaction kinetics of PS conversion. This can be explained by the fact that  $Zn_{0.875}Co_2O_4$  possesses stronger binding energies with  $Li_2S_x$  via density functional theory calculations, relative to  $ZnCo_2O_4$  without Zn vacancies. As a result, lithium-sulfur battery with an extremely high loading can be achieved, which delivered a stable cycle performance and high areal

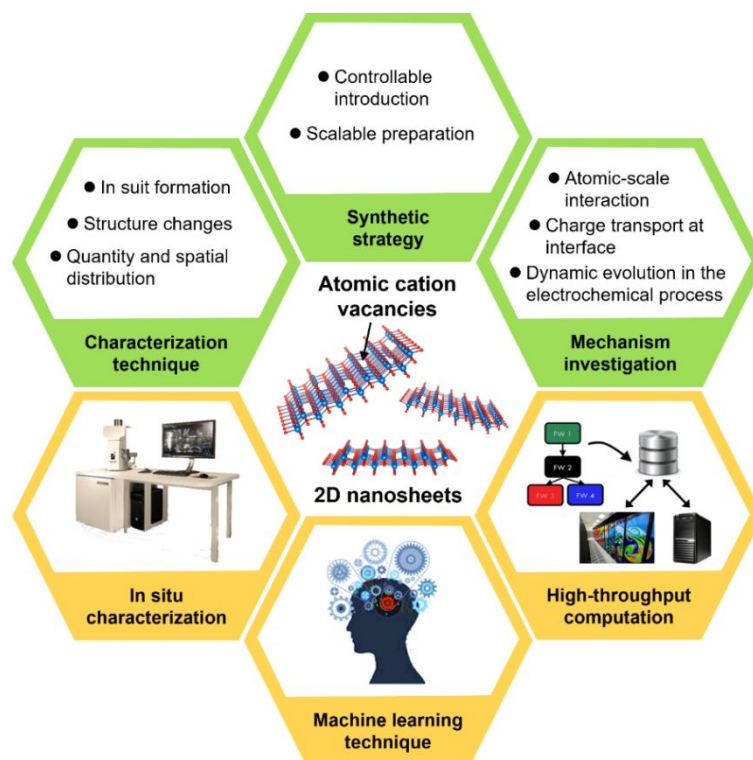


**Fig. 13 The challenges and perspectives for atomic cation-vacancy engineering of 2D nanosheets in energy-related applications.** The challenges of cation-vacancy engineering of 2D nanosheets still retain in the synthetic strategy, characterization technique, and mechanism investigation. The research directions of in situ characterization, machine learning technique and high-throughput computation are promising for cation-deficient 2D nanosheets in energy-related systems in the future.

capacity.

### 3.2.3 Electrocatalysis

Intentional creation of atomic cation vacancies has been explored to increase the electrocatalytic activity of 2D nanosheets by activation of the inert basal plane,<sup>69</sup> enhancement of electron-transferring properties,<sup>70,110</sup> and regulation of favorable atomic strain.<sup>49</sup> Ding et al. theoretically investigated that Mo vacancies can activate the inert basal plane of MoSe<sub>2</sub> for HER (Fig. 11a).<sup>69</sup> The most prominent electrocatalytic activities were experimentally demonstrated for 2D MoSe<sub>2</sub> nanosheets with Mo vacancies (Fig. 11b). In addition, they demonstrated that incorporation of Mo vacancies yielded additional electronic states in the vicinity of Fermi level, thus benefiting enhanced electron-transferring properties for MoSe<sub>2</sub> (Fig. 11c). Due to identifiability of concentration of atomic cation vacancies compared with other types of vacancies, Chhowalla et al. found the HER activities of cation vacancies are strongly dependent on the local atomic strains.<sup>49</sup> The atomic strain near the Mo vacancies is thermodynamically favorable for hydrogen adsorption, which is essential for improving the HER catalytic activities of single layer MoS<sub>2</sub> nanosheets.<sup>111</sup>

The cation vacancies also provide abundant anchoring sites to confine single atoms on nanosheets for high electrocatalytic stability.<sup>109,112,113</sup> Taking electrochemical N<sub>2</sub> reduction reaction (NRR) as an example, under ambient conditions, the low selectivity and poor resistance make them uncompetitive for the synthesis of ammonia in comparison to the industrial Haber-Bosch process.<sup>114</sup> Tan's team reported cation-vacancy Mo<sub>2</sub>CT<sub>x</sub> nanosheets modified

with Ru atoms (Ru-Mo<sub>2</sub>CT<sub>x</sub>) as electrocatalysts toward NRR.<sup>109</sup> Ru-Mo<sub>2</sub>CT<sub>x</sub> showed excellent stability and negligible degradation in the process of recycling electrolysis test (Fig. 11d). Density functional theory (DFT) simulations revealed that Ru 3d has a stronger hybridization with adatom N 2p orbitals than Mo 3d orbitals around the Fermi level (Fig. 11e). Besides, a stronger electronic interaction between Ru sites and \*N<sub>2</sub> than Mo sites was shown during NRR process, (Fig. 11f), which accounts for the NRR durability of Ru-Mo<sub>2</sub>CT<sub>x</sub>.

Moreover, different cation vacancies may play different roles in promoting electrocatalytic properties. For example, introduction of divalent metal (M<sup>2+</sup>) and trivalent metal (M<sup>3+</sup>) cation vacancies can enhance electrocatalytic stability and activity, respectively.<sup>79</sup> The existence of M<sup>2+</sup> vacancies could accelerate the evolution of surface active phases and optimize the binding energies of intermediates on the catalyst surface, thereby boosting the oxygen evolution reaction (OER) activity (Fig. 11g). While, whereas M<sup>3+</sup> vacancies could relieve lattice distortions and dramatically mitigate metal dissolution during OER process, resulting in enhanced OER durability (Fig. 11h). The research on different kinds of cation vacancies is a cutting-edge strategy for the development of highly active and stable electrocatalysts.

### 3.2.4 Photocatalysis

Although 2D nanosheets have been extensively investigated as photocatalysts, the main drawback, including the fast recombination of photogenerated electrons and holes, had hindered their practical applications.<sup>115-117</sup> The introduction of atomic cation vacancies with-

in the 2D photocatalysts could effectively inhibit the negative effect and improve photocatalytic performance. Taking GCN, a typical 2D photocatalyst, as an example,<sup>118,119</sup> C vacancies in GCN nanosheets could generate unpaired electrons around adjacent N atoms and attract electrons from external substances, which further modify the electronic structure and thus improve the photocatalytic ability of GCN nanosheets.<sup>24</sup> For instance, Zhang's group found that bisphenol A could be effectively removed by GCN-Vc via the photocatalytic degradation process (Fig. 12a), and the photocatalytic degradation kinetic constant of GCN-Vc is around 2 times larger than that of pristine GCN (Fig. 12b).<sup>24</sup> Besides, Guan et al. found that GCN-Vc was endowed with a superior photocatalytic hydrogen evolution rate, which was 18.3 times higher than that of pristine GCN (Fig. 12c).<sup>95</sup>

These remarkable performance improvements encouraged researchers to study the intrinsic photocatalytic properties of GCN-Vc and underlying atomic mechanisms associated with the C vacancies, which benefit from a good research platform of GCN nanosheets with atomic C vacancies. Typically, Shen and co-workers studied the beneficial role of C vacancies in GCN-Vc for CO<sub>2</sub> photoreduction (Fig. 12d).<sup>50</sup> The strengthened PL emission peak (Fig. 12e) and enhanced transient photocurrent response (Fig. 12f) in GCN-Vc are due to that C vacancies, widening the band gap and boosting the photoinduced charge carrier concentration (Fig. 12g). Besides, abundant reactive oxygen species, such as singlet oxygen and superoxide radicals, were produced to synergistically benefit the electron-involved photocatalytic reactions for CO<sub>2</sub> photoreduction

**Table 1** Summary of the synthesis methods, characterization techniques and tunable properties for the investigated 2D materials.

2D materials	Cation vacancy types	Synthesis methods	Characterization techniques	Tunable properties
Ti <sub>0.87</sub> O <sub>2</sub> nanosheets <sup>40</sup>	Ti atomic vacancies	Wet-chemistry	HAADF-STEM, XAFS	Li-S, Li-Se and Na-Se batteries (long-term cycling stability)
δ-MnO <sub>2</sub> nanosheets <sup>41</sup>	Mn vacancies	Wet-chemistry	XAS, X-ray scattering, PDF analysis	Supercapacitor (specific capacitance, charge transfer resistance and cycling stability)
δ-FeOOH nanosheets <sup>53</sup>	Fe vacancies	Wet-chemistry	HRTEM	HER and OER (catalytic active centers)
CoSe <sub>2</sub> nanosheets <sup>48</sup>	VCo'' vacancies	Wet-chemistry	PAS, XAFS	Water oxidation (activity and durability)
MoSe <sub>2</sub> nanosheets <sup>70</sup>	Mo vacancies	Ion/electron beam irradiation	Raman, ESR, XPS, HRTEM	HER (catalytic active sites and electrocatalytic capacity)
MoS <sub>2</sub> nanosheets <sup>49</sup>	Mo vacancies	Ion/electron beam irradiation	HAADF-STEM, Raman, PL	HER (charge-transfer kinetics)
TiS <sub>2</sub> nanosheets <sup>61</sup>	Ti vacancies	Thermal anneal	EPR, XPS	Lithium-ion, sodium-ion and potassium-ion batteries (cycle ability and kinetic performance)
CoFe LDHs nanosheets <sup>76</sup>	Co and Fe vacancies	Wet-chemistry	HRTEM, XAS	OER (electrocatalytic activity)
NiFe LDHs nanosheets <sup>42</sup>	Ni and Fe vacancies	Selective etching	XPS	OER (electrocatalytic activity)
NiCu LDH nanosheets <sup>120</sup>	Cu vacancies	Selective etching	HRTEM, XPS	OER (long-term stability and improved kinetics)
Monolayer Ti <sub>3</sub> C <sub>2</sub> T <sub>x</sub> flakes <sup>83</sup>	Ti vacancies	Selective etching	HAADF-STEM	2D electronic device (metallic conductivity)
Mo <sub>1.33</sub> C MXene <sup>39</sup>	Al and Sc vacancies	Selective etching	HAADF-STEM	Supercapacitor (conductivity and volumetric capacitance)
Ti <sub>3-x</sub> C <sub>2</sub> T <sub>y</sub> MXene <sup>62</sup>	Ti vacancies	Selective etching	HAADF-STEM, XAS	CO <sub>2</sub> functionalization (selectivity)
Graphene <sup>46</sup>	C vacancies	Ion/electron beam irradiation	HRTEM	/
Hexagonal boron nitride <sup>47</sup>	Boron monovacancies	Ion/electron beam irradiation	Aberration corrected HRTEM	/
Graphitic carbon nitride <sup>50</sup>	C vacancies	Selective etching	TEM, XPS, ESR	CO <sub>2</sub> photocatalytic reduction (CO <sub>2</sub> -to-CO conversion rate)

(Fig. 12h).

#### 4. Conclusions and perspectives

In this review, we have summarized the recent progress in synthesis methods and characterization techniques of cation vacancies in various 2D cation-deficient nanosheets and applications of such 2D nanosheets in various energy-related systems such as metal ion batteries, lithium-sulfur batteries, electrocatalysis, and photocatalysis (Table 1). The 2D nanosheet is an ideal platform to create cation vacancies due to its unique properties. By introducing cation vacancies, 2D nanosheets can be provided with additional sites, open channels and regulated electronic structures to achieve improved or unprecedented features. Although great advances have been achieved in the preparation, characterization, and application of 2D nanosheets with cation vacancies, there are still some challenges that are worthy of our further exploration and investigation (Fig. 13).

Reasonable and scalable methods should be developed to controllably generate cation vacancies in 2D nanosheets. Especially, the techniques of controllable mass production of cation vacancies in diverse 2D nanosheet systems are very significant toward the commercial scale. In addition, the cost of introducing cation vacancies in 2D nanosheets should also be taken into account. Therefore, developing more low-cost, efficient and eco-friendly methods to construct cation vacancies on 2D nanosheets is highly needed in the future. At the same time, the precise design of cation-vacancy engineering in 2D materials is critical to investigate their performance and stability. At present, there are some difficulties in efficiently introducing cation vacancies in targeted regions, which results in our limited understanding of how cation vacancies affect material properties. 2D cation-vacancy nanosheets need to be precisely designed at the atomic scale according to requirements in order to achieve tailored preparation. There are possible approaches to achieve this goal including the synthesis of high-quality 2D nanosheets, the designation of certain chemical reactions for the introduction of cation vacancies, and precise control of the preparation conditions of cation vacancies in various 2D materials.<sup>121-123</sup> However, it is still difficult to detect the quantity and spatial distribution of cation vacancies in 2D nanosheets with standard characterization techniques. Considering the probable inhomogeneity of the existence of cation vacancy, it is essential to gain an in-depth understanding of the vacancy distribution, especially to acquire its intrinsic effect on the performance for energy storage and conversion. Therefore, more attention should be paid to the development of powerful characterization techniques in the future. In addition, the atomic-scale mechanism of cation vacancies in 2D nanosheets for their improved electrochemical performance is not clear yet. Although some works have revealed the role of cation vacancies as additional sites before or after the reaction, we do not still know its dynamic evolution in the electrochemical process. Advanced in situ characterizations such as in situ TEM and X-ray absorption spectroscopy, are promising to reflect the real-time changes of the vacancy structure during the reaction process. A novel DFT (e.g., high-throughput computation) and machine learning hybrid computation method might track the interaction changes and charge transport at the deficient nanosheet

interfaces, which is also suitable for investigating the atomic-scale mechanism of cation-deficient nanosheets in energy storage and conversion systems.

Overall, the recent progress has definitely made us expect a promising future of 2D cation-deficient nanosheets in energy-related applications. Considering that cation-vacancy engineering has become a universal approach for designing 2D materials, vast other materials will continue to be explored. With the development of advanced in situ techniques, the role of cation vacancies in 2D materials will be further understood at the atomic level. The cation-vacancy engineering strategy of 2D nanosheets is expected to be widely applied in many other applications not limited to the above to solve the social necking problems.

#### Author contributions

**C. Liu:** Conceptualization, Visualization, Writing - original draft, Writing - review & editing. **Y. Liu:** Visualization, Writing - original draft, Writing - review & editing. **R. Ma:** Writing - review & editing. **T. Sasaki:** Funding acquisition, Writing - review & editing. **X. Wang:** Writing - review & editing. **P. Xiong:** Conceptualization, Funding acquisition, Writing - review & editing. **J. Zhu:** Supervision, Funding acquisition, Writing - review & editing.

#### Conflicts of interest

There are no conflicts to declare.

#### Acknowledgements

P. Xiong and J. Zhu acknowledge the financial supported by the Natural Science Foundation of China (No. 22179062, 52125202, 51902161, and U2004209). P. Xiong acknowledges the financial support by the Fundamental Research Funds for the Central Universities (No. 30922010303). R. Ma and T. Sasaki acknowledge the support from WPI-MANA, Ministry of Education, Culture, Sports, Science and Technology, Japan and CREST of the Japan Science and Technology Agency (JST) (No. JPMJCR17N1).

#### References

- 1 K. S. Novoselov, A. K. Geim, S. V. Morozov, D.-e. Jiang, Y. Zhang, S. V. Dubonos, I. V. Grigorieva and A. A. Firsov, Electric field effect in atomically thin carbon films, *Science*, 2004, **306**, 666-669.
- 2 S. Manzeli, D. Ovchinnikov, D. Pasquier, O. V. Yazyev and A. Kis, 2D transition metal dichalcogenides, *Nat. Rev. Mater.*, 2017, **2**, 1-15.
- 3 R. Ma and T. Sasaki, Nanosheets of oxides and hydroxides: ultimate 2D charge-bearing functional crystallites, *Adv. Mater.*, 2010, **22**, 5082-5104.
- 4 P. Xiong, R. Ma, G. Wang and T. Sasaki, Progress and perspective on two-dimensional unilamellar metal oxide nanosheets and tailored nanostructures from them for electrochemical energy storage, *Energy Storage Mater.*, 2019, **19**, 281-298.

- 5 R. Ma, T. Sasaki, Two-dimensional oxide and hydroxide nanosheets: controllable high-quality exfoliation, molecular assembly, and exploration of functionality, *Acc. Chem. Res.*, 2015, **48**, 136-143.
- 6 S. Veeralingam, S. S. Gunasekaran and S. Badhulika, Bifunctional NiFe LDH as a piezoelectric nanogenerator and asymmetric pseudo-supercapacitor. *Mater. Chem. Front.*, 2022, **6**, 2297-2308.
- 7 B. Anasori, M. R. Lukatskaya and Y. Gogotsi, 2D metal carbides and nitrides (MXenes) for energy storage, *Nat. Rev. Mater.*, 2017, **2**, 1-17.
- 8 X. Zhong, D. Wang, J. Sheng, Z. Han, C. Sun, J. Tan, R. Gao, W. Lv, X. Xu, G. Wei, X. Zou and G. Zhou, Freestanding and sandwich MXene-based cathode with suppressed lithium polysulfides shuttle for flexible lithium-sulfur batteries. *Nano Lett.*, 2022, **22**, 1207-1216.
- 9 M. D. Stoller, S. Park, Y. Zhu, J. An and R. S. Ruoff, Graphene-based ultracapacitors, *Nano Lett.*, 2008, **8**, 3498-3502.
- 10 H. Wang, X. Xiao, S. Liu, C.-L. Chiang, X. Kuai, C.-K. Peng, Y.-C. Lin, X. Meng, J. Zhao, J. Choi, Y.-G. Lin, J.-M. Lee and L. Gao, Structural and electronic optimization of MoS<sub>2</sub> edges for hydrogen evolution, *J. Am. Chem. Soc.*, 2019, **141**, 18578-18584.
- 11 P. Xiong, Y. Wu, Y. Liu, R. Ma, T. Sasaki, X. Wang and J. Zhu, Two-dimensional organic-inorganic superlattice-like heterostructures for energy storage applications, *Energy Environ. Sci.*, 2020, **13**, 4834-4853.
- 12 P. Xiong, X. Zhang, F. Zhang, D. Yi, J. Zhang, B. Sun, H. Tian, D. Shanmukaraj, T. Rojo, M. Armand, R. Ma, T. Sasaki and G. Wang, Two-dimensional unilamellar cation-deficient metal oxide nanosheet superlattices for high-rate sodium ion energy storage, *ACS Nano*, 2018, **12**, 12337-12346.
- 13 P. Xiong, R. Ma, N. Sakai and T. Sasaki, Genuine unilamellar metal oxide nanosheets confined in a superlattice-like structure for superior energy storage, *ACS Nano*, 2018, **12**, 1768-1777.
- 14 P. Xiong, F. Zhang, X. Zhang, S. Wang, H. Liu, B. Sun, J. Zhang, Y. Sun, R. Ma, Y. Bando, C. Zhou, Z. Liu, T. Sasaki and G. Wang, Strain engineering of two-dimensional multilayered heterostructures for beyond-lithium-based rechargeable batteries, *Nat. Commun.*, 2020, **11**, 3297.
- 15 P. Xiong, X. Zhang, H. Wan, S. Wang, Y. Zhao, J. Zhang, D. Zhou, W. Gao, R. Ma, T. Sasaki and G. Wang, Interface modulation of two-dimensional superlattices for efficient overall water splitting, *Nano Lett.*, 2019, **19**, 4518-4526.
- 16 J. Xu, X. Cui, N. Liu, Y. Chen and H. W. Wang, Structural engineering of graphene for high-resolution cryo-electron microscopy, *SmartMat*, 2021, **2**, 202-212.
- 17 Z. Teng, N. Yang, H. Lv, S. Wang, M. Hu, C. Wang, D. Wang and G. Wang, Edge-functionalized g-C<sub>3</sub>N<sub>4</sub> nanosheets as a highly efficient metal-free photocatalyst for safe drinking water, *Chem*, 2019, **5**, 664-680.
- 18 X. Zhang, Z. Lai, C. Tan and H. Zhang, Solution-processed two-dimensional MoS<sub>2</sub> nanosheets: preparation, hybridization, and applications, *Angew. Chem., Int. Ed.*, 2016, **55**, 8816-8838.
- 19 Y. Chen, Z. Lai, X. Zhang, Z. Fan, Q. He, C. Tan, H. Zhang, Phase engineering of nanomaterials, *Nat. Rev. Chem.*, 2020, **4**, 243-256.
- 20 H. Wang, L. Zhang, K. Wang, X. Sun and W. Wang, Enhanced photocatalytic CO<sub>2</sub> reduction to methane over WO<sub>3</sub>·0.33H<sub>2</sub>O via Mo doping, *Appl. Catal. B-Environ.*, 2019, **243**, 771-779.
- 21 Y. Zhang, L. Jiao, W. Xu, Y. Chen, Y. Wu, H. Yan, W. Gu and C. Zhu, Defect-rich and ultrathin nitrogen-doped carbon nanosheets with enhanced peroxidase-like activity for the detection of urease activity and fluoride ion, *Chin. Chem. Lett.*, 2022, **33**, 1317-1320.
- 22 B. Sun, D. Fan, X. Chen, Z. Li, W. Zhou and Y. Du, Heteroatom-induced domain electrostatic potential difference in ZnIn<sub>2</sub>S<sub>4</sub> nanosheets for efficient charge separation and boosted photocatalytic overall water splitting, *Mater. Chem. Front.*, 2022, **6**, 1795-1802.
- 23 Y. Zhao, J. Wan, H. Yao, L. Zhang, K. Lin, L. Wang, N. Yang, D. Liu, L. Song, J. Zhu, L. Gu, L. Liu, H. Zhao, Y. Li and D. Wang, Few-layer graphdiyne doped with sp-hybridized nitrogen atoms at acetylenic sites for oxygen reduction electrocatalysis, *Nat. Chem.*, 2018, **10**, 924-931.
- 24 X. Liang, G. Wang, X. Dong, G. Wang, H. Ma and X. Zhang, Graphitic carbon nitride with carbon vacancies for photocatalytic degradation of bisphenol A, *ACS Appl. Nano Mater.*, 2018, **2**, 517-524.
- 25 P. Gao, Z. Chen, Y. Gong, R. Zhang, H. Liu, P. Tang, X. Chen, S. Passerini and J. Liu, The role of cation vacancies in electrode materials for enhanced electrochemical energy storage: synthesis, advanced characterization, and fundamentals, *Adv. Energy Mater.*, 2020, **10**, 1903780.
- 26 A. Zandiatashbar, G.-H. Lee, S.J. An, S. Lee, N. Mathew, M. Terrones, T. Hayashi, C.R. Picu, J. Hone and N. Koratkar, Effect of defects on the intrinsic strength and stiffness of graphene, *Nat. Commun.*, 2014, **5**, 1-9.
- 27 J.-H. Chen, L. Li, W. G. Cullen, E. D. Williams and M. S. Fuhrer, Tunable Kondo effect in graphene with defects, *Nat. Phys.*, 2011, **7**, 535-538.
- 28 R. Meshkian, M. Dahlqvist, J. Lu, B. Wickman, J. Halim, J. Thörnberg, Q. Tao, S. Li, S. Intikhab, J. Snyder, M.W. Barsoum, M. Yildizhan, J. Palisaitis, L. Hultman, P. O. Å. Persson and J. Rosen, W-based atomic laminates and their 2D derivative W<sub>1.33</sub>C MXene with vacancy ordering, *Adv. Mater.*, 2018, **30**, 1706409.
- 29 G. Li, G. R. Blake and T. T. Palstra, Vacancies in functional materials for clean energy storage and harvesting: the perfect imperfection, *Chem. Soc. Rev.*, 2017, **46**, 1693-1706.
- 30 H. Yang and L. Chu, MBenes: Two-dimensional transition-metal borides with ordered metal vacancies, *Chin. Chem. Lett.*, 2023, **34**, 106898.
- 31 X.-Q. Xu, R. Xu, X.-B. Cheng, Y. Xiao, H.-J. Peng, H. Yuan and F. Liu, A two-dimension laminar composite protective layer for dendrite-free lithium metal anode. *J. Energy Chem.*, 2021, **56**, 391-394.
- 32 T. Tang, Z. Wang and J. Guan, A review of defect engineering in two-dimensional materials for electrocatalytic hydrogen evolution reaction, *Chinese J. Catal.*, 2022, **43**, 636-678.
- 33 C. Tang and Q. Zhang, Nanocarbon for oxygen reduction electrocatalysis: dopants, edges, and defects, *Adv. Mater.*, 2017, **29**, 1604103.
- 34 D. Yan, Y. Li, J. Huo, R. Chen, L. Dai and S. Wang, Defect chemistry of nonprecious-metal electrocatalysts for oxygen reactions, *Adv. Mater.*, 2017, **29**, 1606459.
- 35 L. Dai, F. Yao, L. Yu, C. Fang, J. Li, L. Xue, S. Zhang, P. Xiong, Y. Fu, J. Sun and J. Zhu, Boosting alkaline hydrogen evolution on stoichiometric molybdenum carbonitride via an interstitial vacancy-elimination strategy, *Adv. Energy Mater.*, 2022, **12**, 2200974.
- 36 H. Song, F. Liu and M. Luo, Insights into the stable and fast lithium storage performance of oxygen-deficient LiV<sub>3</sub>O<sub>8</sub> nanosheets, *Nano Res.*, 2021, **14**, 814-822.
- 37 C. Sun, P. Wang, H. Wang, C. Xu, J. Zhu, Y. Liang, Y. Su, Y. Jiang, W. Wu, E. Fu and G. Zou, Defect engineering of molybdenum disulfide through ion irradiation to boost hydrogen evolution reaction performance, *Nano Res.*, 2019, **12**, 1613-1618.
- 38 I. Persson, A. El Ghazaly, Q. Tao, J. Halim, S. Kota, V. Darakchieva, J. Palisaitis, M. W. Barsoum, J. Rosen and P. O. Persson, Tailoring structure, composition, and energy storage properties of MXenes from selective etching of in-plane, chemically ordered MAX phases, *Small*, 2018, **14**, 1703676.

- 39 Q. Tao, M. Dahlqvist, J. Lu, S. Kota, R. Meshkian, J. Halim, J. Palisaitis, L. Hultman, M. W. Barsoum, P. O. Å. Persson and J. Rosen, Two-dimensional  $\text{Mo}_{1.33}\text{C}$  MXene with divacancy ordering prepared from parent 3D laminate with in-plane chemical ordering, *Nat. Commun.*, 2017, **8**, 14949.
- 40 P. Xiong, F. Zhang, X. Zhang, Y. Liu, Y. Wu, S. Wang, J. Safaei, B. Sun, R. Ma, Z. Liu, Y. Bando, T. Sasaki, X. Wang, J. Zhu and G. Wang, Atomic-scale regulation of anionic and cationic migration in alkali metal batteries, *Nat. Commun.*, 2021, **12**, 4184.
- 41 P. Gao, P. Metz, T. Hey, Y. Gong, D. Liu, D. D. Edwards, J. Y. Howe, R. Huang and S. T. Misture, The critical role of point defects in improving the specific capacitance of  $\delta\text{-MnO}_2$  nanosheets, *Nat. Commun.*, 2017, **8**, 1-10.
- 42 Y. Wang, M. Qiao, Y. Li and S. Wang, Tuning surface electronic configuration of NiFe LDHs nanosheets by introducing cation vacancies (Fe or Ni) as highly efficient electrocatalysts for oxygen evolution reaction, *Small*, 2018, **14**, 1800136.
- 43 B. Liu, S. Zhan, J. Du, X. Yang, Y. Zhao, L. Li, J. Wan, Z.-J. Zhao, J. Gong, N. Yang, R. Yu and D. Wang, Revealing the mechanism of sp-N doping in graphdiyne for developing site-defined metal-free catalysts, *Adv. Mater.*, 2022, 2206450.
- 44 Y. Zhao, N. Yang, H. Yao, D. Liu, L. Song, J. Zhu, S. Li, L. Gu, K. Lin and D. Wang, Stereodefined codoping of sp-N and S atoms in few-layer graphdiyne for oxygen evolution reaction, *J. Am. Chem. Soc.*, 2019, **141**, 7240-7244.
- 45 J. Xiong, J. Di, J. Xia, W. Zhu and H. Li, Surface defect engineering in 2D nanomaterials for photocatalysis, *Adv. Funct. Mater.*, 2018, **28**, 1801983.
- 46 A. Hashimoto, K. Suenaga, A. Gloter, K. Urita and S. Iijima, Direct evidence for atomic defects in graphene layers, *Nature*, 2004, **430**, 870-873.
- 47 C. Jin, F. Lin, K. Suenaga and S. Iijima, Fabrication of a freestanding boron nitride single layer and its defect assignments, *Phys. Rev. Lett.*, 2009, **102**, 195505.
- 48 Y. Liu, H. Cheng, M. Lyu, S. Fan, Q. Liu, W. Zhang, Y. Zhi, C. Wang, C. Xiao, S. Wei, B. Ye and Y. Xie, Low overpotential in vacancy-rich ultrathin  $\text{CoSe}_2$  nanosheets for water oxidation, *J. Am. Chem. Soc.*, 2014, **136**, 15670-15675.
- 49 J. Yang, Y. Wang, M. J. Lagos, V. Manichev, R. Fullon, X. Song, D. Voiry, S. Chakraborty, W. Zhang, P. E. Batson, L. Feldman, T. Gustafsson and M. Chhowalla, Single atomic vacancy catalysis, *ACS Nano*, 2019, **13**, 9958-9964.
- 50 M. Shen, L. Zhang, M. Wang, J. Tian, X. Jin, L. Guo, L. Wang and J. Shi, Carbon-vacancy modified graphitic carbon nitride: enhanced  $\text{CO}_2$  photocatalytic reduction performance and mechanism probing, *J. Mater. Chem. A*, 2019, **7**, 1556-1563.
- 51 T. Sasaki, M. Watanabe, H. Hashizume, H. Yamada and H. Nakazawa, Macromolecule-like aspects for a colloidal suspension of an exfoliated titanate. Pairwise association of nanosheets and dynamic reassembling process initiated from it, *J. Am. Chem. Soc.*, 1996, **118**, 8329-8335.
- 52 T. Sasaki, Fabrication of nanostructured functional materials using exfoliated nanosheets as a building block, *J. Ceram. Soc. Jpn.*, 2007, **115**, 9-16.
- 53 B. Liu, Y. Wang, H. Q. Peng, R. Yang, Z. Jiang, X. Zhou, C. S. Lee, H. Zhao and W. Zhang, Iron vacancies induced bifunctionality in ultrathin ferroxhyte nanosheets for overall water splitting, *Adv. Mater.*, 2018, **30**, 1803144.
- 54 Y. Ma, B. Qiu, J. Zhang and M. Xing, Vacancy engineering of ultrathin 2D materials for photocatalytic  $\text{CO}_2$  reduction, *ChemNanoMat*, 2021, **7**, 368-379.
- 55 A. A. AbdelHamid, Y. Yu, J. Yang and J. Y. Ying, Generalized synthesis of metal oxide nanosheets and their application as Li-ion battery anodes, *Adv. Mater.*, 2017, **29**, 1701427.
- 56 W. Chen, R. Zhang, Y. Sun, J. Wang, Y. Fan and B. Liu, Preparation, properties, and electronic applications of 2D  $\text{Bi}_2\text{O}_2\text{Se}$ , *Adv. Powder Mater.*, 2023, **2**, 100080.
- 57 T. Sasaki and M. Watanabe, Osmotic swelling to exfoliation. Exceptionally high degrees of hydration of a layered titanate, *J. Am. Chem. Soc.*, 1998, **120**, 4682-4689.
- 58 M. Ohwada, K. Kimoto, T. Mizoguchi, Y. Ebina and T. Sasaki, Atomic structure of titania nanosheet with vacancies, *Sci. Rep.*, 2013, **3**, 1-5.
- 59 T. Maluangnont, K. Matsuba, F. Geng, R. Ma, Y. Yamauchi and T. Sasaki, Osmotic swelling of layered compounds as a route to producing high-quality two-dimensional materials. A comparative study of tetramethylammonium versus tetrabutylammonium cation in a lepidocrocite-type titanate, *Chem. Mater.*, 2013, **25**, 3137-3146.
- 60 F. Geng, R. Ma, Y. Ebina, Y. Yamauchi, N. Miyamoto and T. Sasaki, Gigantic swelling of inorganic layered materials: a bridge to molecularly thin two-dimensional nanosheets, *J. Am. Chem. Soc.*, 2014, **136**, 5491-5500.
- 61 T. Liu, X. Zhang, M. Xia, H. Yu, N. Peng, C. Jiang, M. Shui, Y. Xie, T.-F. Yi and J. Shu, Functional cation defects engineering in  $\text{TiS}_2$  for high-stability anode, *Nano Energy*, 2020, **67**, 104295.
- 62 D. Zhao, Z. Chen, W. Yang, S. Liu, X. Zhang, Y. Yu, W.-C. Cheong, L. Zheng, F. Ren, G. Ying, X. Cao, D. Wang, Q. Peng, G. Wang and C. Chen, MXene ( $\text{Ti}_3\text{C}_2$ ) vacancy-confined single-atom catalyst for efficient functionalization of  $\text{CO}_2$ , *J. Am. Chem. Soc.*, 2019, **141**, 4086-4093.
- 63 Y. Chen, Z. Fan, Z. Zhang, W. Niu, C. Li, N. Yang, B. Chen and H. Zhang, Two-dimensional metal nanomaterials: synthesis, properties, and applications, *Chem. Rev.*, 2018, **118**, 6409-6455.
- 64 Z. Lin, B. R. Carvalho, E. Kahn, R. Lv, R. Rao, H. Terrones, M. A. Pimenta and M. Terrones, Defect engineering of two-dimensional transition metal dichalcogenides, *2D Mater.*, 2016, **3**, 022002.
- 65 H. Li, C. Tsai, A. L. Koh, L. Cai, A. W. Contryman, A. H. Fragapane, J. Zhao, H. S. Han, H. C. Manoharan, F. Abild-Pedersen, J. K. Nørskov and X. Zheng, Activating and optimizing  $\text{MoS}_2$  basal planes for hydrogen evolution through the formation of strained sulphur vacancies, *Nat. Mater.*, 2016, **15**, 48-53.
- 66 J. Hong, Z. Hu, M. Probert, K. Li, D. Lv, X. Yang, L. Gu, N. Mao, Q. Feng, L. Xie, J. Zhang, D. Wu, Z. Zhang, C. Jin, W. Ji, X. Zhang, J. Yuan and Z. Zhang, Exploring atomic defects in molybdenum disulphide monolayers, *Nat. Commun.*, 2015, **6**, 6293.
- 67 Y. Xu, L. Wang, X. Liu, S. Zhang, C. Liu, D. Yan, Y. Zeng, Y. Pei, Y. Liu and S. Luo, Monolayer  $\text{MoS}_2$  with S vacancies from interlayer spacing expanded counterparts for highly efficient electrochemical hydrogen production, *J. Mater. Chem. A*, 2016, **4**, 16524-16530.
- 68 Y. L. Huang, W. Chen and A. T. Wee, Two-dimensional magnetic transition metal chalcogenides, *SmartMat*, 2021, **2**, 139-153.
- 69 D. Gao, B. Xia, Y. Wang, W. Xiao, P. Xi, D. Xue and J. Ding, Dual-native vacancy activated basal plane and conductivity of  $\text{MoSe}_2$  with high-efficiency hydrogen evolution reaction, *Small*, 2018, **14**, 1704150.
- 70 B. Xia, T. Wang, X. Jiang, T. Zhang, J. Li, W. Xiao, P. Xi, D. Gao, D. Xue and J. Ding,  $\text{Ar}^{2+}$  beam irradiation-induced multivacancies in  $\text{MoSe}_2$  nanosheet for enhanced electrochemical hydrogen evolution, *ACS Energy Lett.*, 2018, **3**, 2167-2172.
- 71 Y. Li, R. Zhang, W. Zhou, X. Wu, H. Zhang and J. Zhang, Hierarchical  $\text{MoS}_2$  hollow architectures with abundant Mo vacancies for efficient sodium storage, *ACS Nano*, 2019, **13**, 5533-5540.
- 72 Y. Yin, X. Kang and B. Han, Two-dimensional materials: synthesis and applications in the electro-reduction of carbon dioxide, *Chem. Synth.*, 2022, **2**, 19.
- 73 J. P. Thiruraman, P. Masih Das and M. Drndić, Irradiation of transition metal dichalcogenides using a focused ion beam:

- controlled single-atom defect creation, *Adv. Funct. Mater.*, 2019, **29**, 1904668.
- 74 F. Cheng, J. Shen, B. Peng, Y. Pan, Z. Tao and J. Chen, *Nat. Chem.*, 2011, **3**, 79-84.
- 75 S. Gao, L. Wang, C. Zhao, A. Wang, X. Lang, Z. Liu and W. Wang, A review of the synergistic effect of multi-coordination crystal fields on electrocatalysts. *Mater. Chem. Front.*, 2021, **5**, 6718-6734.
- 76 R. Liu, Y. Wang, D. Liu, Y. Zou and S. Wang, Water-plasma-enabled exfoliation of ultrathin layered double hydroxide nanosheets with multivacancies for water oxidation, *Adv. Mater.*, 2017, **29**, 1701546.
- 77 Y. Wang, Y. Zhang, Z. Liu, C. Xie, S. Feng, D. Liu, M. Shao and S. Wang, Layered double hydroxide nanosheets with multiple vacancies obtained by dry exfoliation as highly efficient oxygen evolution electrocatalysts, *Angew. Chem., Int. Ed.*, 2017, **56**, 5867-5871.
- 78 M. Chhowalla, H. S. Shin, G. Eda, L. J. Li, K. P. Loh and H. Zhang, The chemistry of two-dimensional layered transition metal dichalcogenide nanosheets, *Nat. Chem.*, 2013, **5**, 263-275.
- 79 L. Peng, N. Yang, Y. Yang, Q. Wang, X. Xie, D. Sun-Waterhouse, L. Shang, T. Zhang and G. I. N. Waterhouse, Atomic cation-vacancy engineering of NiFe-layered double hydroxides for improved activity and stability towards the oxygen evolution reaction, *Angew. Chem., Int. Ed.*, 2021, **60**, 24612-24619.
- 80 J. Wang, C.-F. Du, Y. Xue, X. Tan, J. Kang, Y. Gao, H. Yu and Q. Yan, MXenes as a versatile platform for reactive surface modification and superior sodium-ion storages, *Exploration*, 2021, **1**, 20210024.
- 81 T. Zhang, L. Zhang and Y. Hou, MXenes: Synthesis strategies and lithium-sulfur battery applications, *eScience*, 2022, **2**, 164-182.
- 82 S. De, S. Acharya, S. Sahoo and G. C. Nayak, Current trends in MXene research: properties and applications, *Mater. Chem. Front.*, 2021, **5**, 7134-7169.
- 83 X. Sang, Y. Xie, M. W. Lin, M. Alhabeb, K. L. Van Aken, Y. Gogotsi, P. R. C. Kent, K. Xiao and R. R. Unocic, Atomic defects in monolayer titanium carbide (Ti<sub>3</sub>C<sub>2</sub>T<sub>x</sub>) MXene, *ACS Nano*, 2016, **10**, 9193-9200.
- 84 J. Halim, J. Palisaitis, J. Lu, J. Thörnberg, E. J. Moon, M. Precner, P. Eklund, P. O. Å. Persson, M. W. Barsoum and J. Rosen, Synthesis of two-dimensional Nb<sub>1.33</sub>C (MXene) with randomly distributed vacancies by etching of the quaternary solid solution (Nb<sub>2/3</sub>Sc<sub>1/3</sub>)<sub>2</sub>AlC MAX phase, *ACS Appl. Nano Mater.*, 2018, **1**, 2455-2460.
- 85 F. Xia, J. Lao, R. Yu, X. Sang, J. Luo, Y. Li and J. Wu, Ambient oxidation of Ti<sub>3</sub>C<sub>2</sub> MXene initialized by atomic defects, *Nanoscale*, 2019, **11**, 23330-23337.
- 86 D. Qu, X. Peng, Y. Mi, H. Bao, S. Zhao, X. Liu and J. Luo, Nitrogen doping and titanium vacancies synergistically promote CO<sub>2</sub> fixation in seawater, *Nanoscale*, 2020, **12**, 17191-17195.
- 87 T. R. Gordon, M. Cargnello, T. Paik, F. Mangolini, R. T. Weber, P. Fornasiero and C. B. Murray, Nonaqueous synthesis of TiO<sub>2</sub> nanocrystals using TiF<sub>4</sub> to engineer morphology, oxygen vacancy concentration, and photocatalytic activity, *J. Am. Chem. Soc.*, 2012, **134**, 6751-6761.
- 88 L. Peng, Z. Xu, Z. Liu, Y. Wei, H. Sun, Z. Li, X. Zhao and C. Gao, An iron-based green approach to 1-h production of single-layer graphene oxide, *Nat. Commun.*, 2015, **6**, 5716.
- 89 J. Chen, Y. Li, L. Huang, C. Li and G. Shi, High-yield preparation of graphene oxide from small graphite flakes via an improved Hummers method with a simple purification process, *Carbon*, 2015, **81**, 826-834.
- 90 D.-Y. Wu and J.-J. Shao, Graphene-based flexible all-solid-state supercapacitors. *Mater. Chem. Front.*, 2021, **5**, 557-583.
- 91 P. Feicht and S. Eigner, Defects in graphene oxide as structural motifs, *ChemNanoMat*, 2018, **4**, 244-252.
- 92 A. W. Robertson and J. H. Warner, Atomic resolution imaging of graphene by transmission electron microscopy, *Nanoscale*, 2013, **5**, 4079-4093.
- 93 P. Niu, L. Zhang, G. Liu and H. M. Cheng, Graphene-like carbon nitride nanosheets for improved photocatalytic activities, *Adv. Funct. Mater.*, 2012, **22**, 4763-4770.
- 94 Y. He, Q. Lei, C. Li, Y. Han, Z. Shi and S. Feng, Defect engineering of photocatalysts for solar-driven conversion of CO<sub>2</sub> into valuable fuels, *Mater. Today*, 2021, **50**, 358-384.
- 95 X. Chen, X. Li, X. Li, H. Lu, L. Wang, Q. Liu, H. Li, J. Ding, H. Wan and G. Guan, Accurate engineering of hexagonal hollow carbon nitride with carbon vacancies: enhanced photocatalytic H<sub>2</sub> evolution and its mechanism, *J. Mater. Chem. A*, 2021, **9**, 20664-20675.
- 96 Y. Zhao, N. Yang, C. Wang, L. Song, R. Yu and D. Wang, Boosting hydrogen evolution reaction on few-layer graphdiyne by sp-N and B co-doping, *APL Mater.*, 2021, **9**, 071102.
- 97 Y. Zhao, J. Wan, N. Yang, R. Yu and D. Wang, sp-Hybridized nitrogen doped graphdiyne for high-performance Zn-air batteries, *Mater. Chem. Front.*, 2021, **5**, 7987-7992.
- 98 X. Li, R. Wang, Y. Yu, X. Wang, T. Gao, W. Lü, T. Yao and B. Song, MOF-derived multi-shelled NiP<sub>2</sub> microspheres as high-performance anode materials for sodium-/potassium-ion batteries, *Adv. Energy Sustainable Res.*, 2022, **3**, 2200010.
- 99 S. Huang, Y. Lv, W. Wen, T. Xue, P. Jia, J. Wang, J. Zhang and Y. Zhao, Three-dimensional hierarchical porous hard carbon for excellent sodium/potassium storage and mechanism investigation, *Mater. Today Energy*, 2021, **20**, 100673.
- 100 J. Zhou and S. Guo, Carbon-based anode materials for potassium-ion batteries: From material, mechanism to performance, *SmartMat*, 2021, **2**, 176-201.
- 101 J. Cao, D. Zhang, R. Chanajaree, Y. Yue, Z. Zeng, X. Zhang and J. Qin, Stabilizing zinc anode via a chelation and desolvation electrolyte additive, *Adv. Powder Mater.*, 2022, **1**, 100007.
- 102 J. Meng, Y. Song, Z. Qin, Z. Wang, X. Mu, J. Wang and X.-X. Liu, Cobalt-nickel double hydroxide toward mild aqueous zinc-ion batteries, *Adv. Funct. Mater.*, 2022, **32**, 2204026.
- 103 Z.W. Seh, Y. Sun, Q. Zhang and Y. Cui, Designing high-energy lithium-sulfur batteries, *Chem. Soc. Rev.*, 2016, **45**, 5605-5634.
- 104 Q. Pang, X. Liang, C. Y. Kwok and L. F. Nazar, Advances in lithium-sulfur batteries based on multifunctional cathodes and electrolytes, *Nat. Energy*, 2016, **1**, 1-11.
- 105 T. Yang, J. Xia, Z. Piao, L. Yang, S. Zhang, Y. Xing and G. Zhou, Graphene-based materials for flexible lithium-sulfur batteries, *ACS Nano*, 2021, **15**, 13901-13923.
- 106 Z. Li, Q. Zhang, L. Hencz, J. Liu, P. Kaghazchi, J. Han, L. Wang and S. Zhang, Multifunctional cation-vacancy-rich ZnCo<sub>2</sub>O<sub>4</sub> polysulfide-blocking layer for ultrahigh-loading Li-S battery, *Nano Energy*, 2021, **89**, 106331.
- 107 X.-B Cheng, C.-Z. Zhao, Y.-X. Yao, H. Liu and Q. Zhang, Recent advances in energy chemistry between solid-state electrolyte and safe lithium-metal anodes, *Chem*, 2019, **5**, 74-96.
- 108 X.-Y. Yue, J. Zhang, J. Bao, Y.-F. Bai, X.-L. Li, S.-Y. Yang, Z.-W. Fu, Z.-H. Wang and Y.-N. Zhou, Sputtered MoN nanolayer as a multifunctional polysulfide catalyst for high-performance lithium-sulfur batteries, *eScience*, 2022, **2**, 329-338.
- 109 W. Peng, M. Luo, X. Xu, K. Jiang, M. Peng, D. Chen, T.-S. Chan and Y. Tan, Spontaneous atomic ruthenium doping in Mo<sub>2</sub>C<sub>x</sub> MXene defects enhances electrocatalytic activity for the nitrogen reduction reaction, *Adv. Energy Mater.*, 2020, **10**, 2001364.
- 110 Y. Liu, C. Ye, S.-N. Zhao, Y. Wu, C. Liu, J. Huang, L. Xue, J. Sun, W. Zhang, X. Wang, P. Xiong and J. Zhu, A dual-site doping

- strategy for developing efficient perovskite oxide electrocatalysts towards oxygen evolution reaction, *Nano Energy*, 2022, **99**, 107344.
- 111 C. Tsai, H. Li, S. Park, J. Park, H. S. Han, J. K. Norskov, X. Zheng and F. Abild-Pedersen, Electrochemical generation of sulfur vacancies in the basal plane of MoS<sub>2</sub> for hydrogen evolution, *Nat. Commun.*, 2017, **8**, 15113.
- 112 Y. Wu, C. Ye, L. Yu, Y. Liu, J. Huang, J. Bi, L. Xue, J. Sun, J. Yang, W. Zhang, X. Wang, P. Xiong and J. Zhu, Soft template-directed interlayer confinement synthesis of a Fe-Co dual single-atom catalyst for Zn-air batteries, *Energy Storage Mater.*, 2022, **45**, 805-813.
- 113 Y. Liu, H. Huang, L. Xue, J. Sun, X. Wang, P. Xiong and J. Zhu, Recent advances in heteroatom doping of perovskite oxides for efficient electrocatalytic reactions, *Nanoscale*, 2021, **13**, 19840-19856.
- 114 S. Zhao, X. Lu, L. Wang, J. Gale and R. Amal, Carbon-based metal-free catalysts for electrocatalytic reduction of nitrogen for synthesis of ammonia at ambient conditions, *Adv. Mater.*, 2019, **31**, e1805367.
- 115 G. Dong, W. Ho, Y. Li and L. Zhang, Facile synthesis of porous graphene-like carbon nitride (C<sub>6</sub>N<sub>9</sub>H<sub>3</sub>) with excellent photocatalytic activity for NO removal, *Appl. Catal. B-Environ.*, 2015, **174-175**, 477-485.
- 116 L. Kong, J. Wang, X. Mu, R. Li, X. Li, X. Fan, P. Song, F. Ma and M. Sun, Porous size dependent g-C<sub>3</sub>N<sub>4</sub> for efficient photocatalysts: Regulation synthesizes and physical mechanism, *Mater. Today Energy*, 2019, **13**, 11-21.
- 117 Y. Wu, P. Xiong, J. Wu, Z. Huang, J. Sun, Q. Liu, X. Cheng, J. Yang, J. Zhu and Y. Zhou, Band engineering and morphology control of oxygen-incorporated graphitic carbon nitride porous nanosheets for highly efficient photocatalytic hydrogen evolution, *Nano-Micro Lett.*, 2021, **13**, 1-12.
- 118 S. Li, G. Dong, R. Hailili, L. Yang, Y. Li, F. Wang, Y. Zeng and C. Wang, Effective photocatalytic H<sub>2</sub>O<sub>2</sub> production under visible light irradiation at g-C<sub>3</sub>N<sub>4</sub> modulated by carbon vacancies, *Appl. Catal. B-Environ.*, 2016, **190**, 26-35.
- 119 J. Sun, F. Yao, L. Dai, J. Deng, H. Zhao, L. Zhang, Y. Huang, Z. Zou, Y. Fu and J. Zhu, Task-specific synthesis of 3D porous carbon nitrides from the cycloaddition reaction and sequential self-assembly strategy toward photocatalytic hydrogen evolution, *ACS Appl. Mater. Interfaces*, 2020, **12**, 40433-40442.
- 120 Y.-S. Xie, Z. Wang, M. Ju, X. Long and S. Yang, Dispersing transition metal vacancies in layered double hydroxides by ionic reductive complexation extraction for efficient water oxidation, *Chemical Science*, 2019, **10**, 8354-8359.
- 121 B. Liu, L. Xu, Y. Zhao, J. Du, N. Yang and D. Wang, Heteroatoms in graphdiyne for catalytic and energy-related applications, *J. Mater. Chem. A*, 2021, **9**, 19298-19316.
- 122 S. Zhan, Y. Zhao, N. Yang and D. Wang, Pore structure of graphdiyne: design, synthesis and application, *Chem. J. Chin. Univ.*, 2021, **42**, 333-348.
- 123 Q. Qi, L. Xu, J. Du, N. Yang and D. Wang, Fabrication and application of graphdiyne-based heterogeneous compositions: from the view of interaction, *Chem. Res. Chin. Univ.*, 2021, **37**, 1158-1175.